Final Report for NAS8-39131 Delivery Order 7

December 16, 1993

W. C. Neely, M.J. Bozak, and J.R. Williams
Space Power Institute
Auburn University, AL 36849

X-ray photoelectron spectroscopy (XPS), Rutherford Back Scattering (RBS) studies of each of sample received were completed . Since low angle X-ray could be performed because instrumentation problems; Auger spectrometry was employed instead. The results of these measurements for each of the samples is discussed in turn:

Results of Analyses

1. Part A0171-IV-80 , OCLI Ag Alloy, As Received.

A. Cresent shaped section

The Auger survey scan showed signatures of Al_2O_3 and SiO_2 located at ca 1400 eV and 1600 eV respectively. Ag was seen at ca 370 eV.

The XPS survey scan also showed signatures of Al_2O_3 and SiO_2. In the XPS these were located between about 75 and about 180 eV. Silver, possibly as AgO was seen near 375 eV.

High resolution XPS scan of the spectral region between 360 eV and 380 eV showed clear evidence of Ag in the form of AgO with characteristic spacing of ca 5 eV between adjacent peaks.

B. Rest of sample (Part A0171-IV-80 , OCLI Ag Alloy, As Received)

An Auger survey scan (No. 4) of this sample showed signature of Al_2O_3 but not of SiO_2.

2. Part A0171-IV-38, Cascade Enhnaced Al, As Received

Auger survey scan of this sample showed SiO_2. signature. XPS survey scan of this sample also has SiO_2. signature.

3. Part A0171-IV-49, Pre-Ox, NCAZ, As Received.

A. Cresent shaped section:

The Auger survey scan of this sample showed Ni, C, O, and Si, located as marked on the spectrum.

The XPS survey scan of this sample also showed Ni and O.

The high-resolution XPS scan of this sample showed that the observed spectrum is characteristic of NiO.

B. Rest of sample (Part A0171-IV-49, Pre-Ox, NCAZ, As Received).

In the Auger survey scan , Ni, Si, S, C, N, and O were seen. Some of the signals were weak; the possible role of contamination cannot be determined by us but should be considered.

The Rutherford backscattering (RBS) measurements on these samples are discussed in turn

1. Part A0171-IV-80 , OCLI Ag Alloy, As Received.

A. Brown section

The RBS data for this sample is attached (Fig. 1). It can be seen that the top 800 A layer is primarily Al_2O_3 with a small amount of Ag. Below this is a 1400 A layer of MgF_2 followed by a 1100 A layer of Ag, then a 300 A layer of Ti and finally the Ni substrate. The RBS spectrum shows the experimental scattering data as the individual points and the simulation based on the above analysis as the solid curve. The peaks corresponding to the various elements are noted on spectrum.

B. Shiny section (Part A0171-IV-80 , OCLI Ag Alloy, As Received)

Here, as seen in Figure 2, the top 1000 A are Al_2O_3 while the nest 1200 A are MgF_2 abd again the next 1100 A are Ag with a 300 A layer of Ti on top of the Ni substrate. Again, the RBS spectrum shows the experimental scattering data as the individual points and the simulation based on the above analysis as the solid curve. The peaks corresponding to the various elements are noted on spectrum.

2. Part A0171-IV-38, Cascade Enhnaced Al, As Received

As shown in Figure 3, the top 1400 A of this sample are SiO_2 followed by 1500 A of Al next to the Ni substrate.
The RBS spectrum shows the experimental scattering data as the individual points and the simulation based on the above analysis as the solid curve. The peaks corresponding to the various elements are noted on spectrum.

3. Part A0171-IV-49, Pre-Ox, NCAZ, As Received.

A. Brown section:

The top 750 A are a mixture of Ni, Cr, Al, Zr, and O in the ratios shown on the spectrum (Fig. 4) Below this is the substrate which appears to be the same ratio of the metals but while O is 1.0 on the top layer it is 0.5 below. This is reasonable finding for an oxidized metal surface. The oxygen found in the bottom layer could be contamination or an incorporated impurity in the original material or could result from penetration of the bulk of the material by atomic oxygen.

B. Shiny section (Part A0171-IV-49, Pre-Ox, NCAZ, As Received).

Again, the elements found are a mixture of Ni, Cr, Al, Zr, and O in the ratios shown on the spectrum (Fig. 5). This is the same composition found in the substrate layer of the brown section and so probably represents unexposed sample.

Thin Films on Beryllium

These samples wee similarly tested using XPS, Auger, and RBS spectrometry. The discussions and conclusions for each set of analyses are shown separately

Auger and XPS Spectrometry Analyses

Conditions of Measurement:

Auger transitions were excited using a 5 kV electron beam with 0.25 μA incident current. The Auger electrons were collected by a hemispherical energy analyzer operating at a fixed retard ratio (FRR) of 20. The AES energy scale was calibrated by setting the Cu(LMM) Auger line on clean copper to exactly 918.7 eV referenced to the Fermi level. The Auger current was collected in V/F mode.

XPS spectra were recorded by a hemispherical energy analyzer operating in the fixed analyzer transmission (FAT) mode with a pass energy of 20 eV. Unmonochromatized Al Kα (1486.6 eV) radiation was used exclusively. The X-ray power was 195 W (13 kV @ 15 mA). The XPS energy scale was calibrated by setting the Ag $3d_{5/2}$ line on clean silver to exactly 368.3 eV referenced to the Fermi level. The photoemission current was collected in pulse count mode. Due to the possibility of sample charging during X-ray irradiation on oxide specimens, we have shifted the energy axis of each XPS spectra to make the C1s peak equal to 284.6 eV, which is a standard hydrocarbon energy used by surface scientists to reference charge-affected materials. The potential measured on a typical sample was of the order of 1-2 V.

Results:

Ta Specimen AO171-IV-73

Side A: AES and XPS were performed on Sides A and B of this specimen. Figure 1 shows the results for Side A. Figure 1(a) is the AES spectrum of the surface. In addition to Ta and O, signals of C, N, Pb, and Al are observed. The C and N are due to gas adsorption from the atmosphere and are universally observed in surface analytical studies of specimens exposed to the atmosphere. The Al and Pb are

contaminants which presumably originate from an external source. Figure 1(b) shows the XPS spectrum from Side A. The Pb signal is clearly evident (Pb has a high probability of excitation in XPS). The surface stoichiometry (atomic %) of Side A determined by XPS from relative elemental sensitivity factors is: Ta: 9.1%, O: 49.8%, C: 40.6%, and Pb: 0.5%. Figure 1(c,d) shows high resolution XPS data taken by scanning over the Ta4f and O1s peaks. There are four Ta4f peaks observed, two strong, high BE features and two weaker, low BE features. Although the BE's of the two weaker peaks are not equal to the BE's for elemental Ta, the peaks have the same energy difference (1.8 eV) and relative peak heights as Ta metal (cf. Appendix A). The difference in BE could be due to errors in charge correction on this side. The pair of high BE peaks at 27.4 eV and 25.7 eV have the same energy difference (1.7 eV) and relative peak areas as to Ta_2O_5, although, once again, the BE's are different; Sarma et al. [1] report 27.6 eV and 26.2 eV for the energies, respectively, for Ta_2O_5. Despite the slight BE difference from elemental Ta and Ta_2O_5, we conclude that the surface contains both elemental Ta and Ta_2O_5 (also cf. Side B, where the high BE components are, within experimental accuracy, equal to those for Ta_2O_5). A four-component deconvolution (Fig. 1(e)) of Ta4f shows that four Gaussian components are successful in modeling the peak shape, with component areas indicating that 16% of the total Ta4f signal originates from Ta metal and 84% originates from Ta_2O_5. The O1s feature for Side A (Fig. 1(d)) provides further evidence for the existence of Ta_2O_5. The O1s feature contains a doublet structure which has been observed in standards (cf. Appendix B) of Ta_2O_5 by Garbassi [2] and Uwamino [3]. A major peak is evident at 529.9 eV and clear evidence of a second, higher BE component is observed near 532.1 eV. A deconvolution of O1s into two states is shown in Fig. 1(f). Garbassi and Uwamino attribute the higher BE component to adsorbed H_2O or OH surface species.

Side B: Figure 2 shows the results for Side B. Figure 2(a) is the AES spectrum of the surface. In addition to Ta and O, signals of C, N, Si, and Al are observed. The C and N are due to gas adsorption from the atmosphere; Al and Si are contaminants which presumably originate from an external source. Figure 2(b) shows the XPS spectrum from Side B. The Si and Al signals are clearly evident. The surface stoichiometry (atomic %) of Side B determined by XPS from relative elemental sensitivity factors is: Ta: 7.8%, O: 66.0%, C: 12.1%, Si: 11.9%, and Al: 2.4%. Figure 2(c, d) shows high resolution XPS data taken by scanning over the Ta4f and O1s peaks. Several features are noteworthy. First, note that the two low BE signals indicative of elemental Ta observed on Side A are negligible on Side B. Second, the high BE pair of Ta4f peaks are measured to be 27.8 eV and 26.1 eV, which are, within experimental accuracy, equal to the literature values for Ta_2O_5. A four component deconvolution (Fig. 2(e)) shows that 3% of the total Ta4f signal originates

from elemental Ta and 97% originates from Ta_2O_5. The O1s feature on Side B (Fig. 2(d)) displays a doublet structure similar to O1s on Side A, but the high BE component has grown (Fig. 2(f)). In summary, Ta_2O_5 has been formed on both sides: there is more oxygen on Side B; and more Ta_2O_5 is present on Side B.

W Specimen AO171-IV-68

Side A: AES and XPS were performed on Sides A and B of this specimen. Figure 3 shows the results for Side A. Figure 1(a) is the AES spectrum of the surface. In addition to W and O, signals of C and N are observed, due to gas adsorption from the atmosphere. We find no extraneous contaminants on the surface of this specimen. Figure 3(b) shows the XPS spectrum from Side A. The surface stoichiometry (atomic %) of Side A determined by XPS from relative elemental sensitivity factors is: W: 22.6%, O: 50.3%, C: 25.1%, N: 2.0%. Figure 3(c,d) shows high resolution XPS data taken by scanning over the W4f and O1s peaks. There are four W4f peaks observed, two weak, high BE features and two stronger, low BE features. Within the experimental uncertainty (0.1 eV) of the measurement, the two stronger lines have BE's equal to elemental W. The peaks also have the same energy difference (2.2 eV) and relative peak heights as W metal (cf. Appendix A). The pair of high BE peaks at 37.5 eV and 35.6 eV are, within experimental error, equal to BE's found in the literature [4-5] for WO_3. Thus, the surface contains both elemental W and WO_3. A four-component deconvolution (Fig. 3(e)) of W4f shows that four Gaussian components are successful in modeling the peak shape, with component areas indicating that 63% of the total W4f signal originates from W metal and 37% originates from WO_3. The O1s feature for Side A (Fig. 3(d)) contains a doublet structure reminiscent of O1s on the Ta specimen. A major peak is evident at 530.5 eV, but the hint of a higher BE component near 532.0 eV is visible. A deconvolution of O1s into two states is shown in Fig. 3(f). Colton et al. [4] report a BE of 530.3 eV for O1s on both WO_2 and WO_3 with no mention of a doublet structure. Fleisch et al. [6] report a broadening of O1s in WO_3 after UV irradiation in a H_2 ambient, which they attribute to formation of hydroxyl groups. It may be that the high BE component is due to adsorbed H_2O or OH groups on the surface, as mentioned above for Ta surfaces.

Side B: Figure 4 shows the results for Side B. Figure 4(a) is the AES spectrum of the surface. In addition to W and O, signals of C, N, and Si are observed. The Si contaminant presumably originates from an external source. Figure 4(b) shows the XPS spectrum from Side B. The Si signals are also evident in XPS. The surface stoichiometry (atomic %) of Side B determined by XPS from relative elemental sensitivity factors is: W: 5.9%, O: 70.6%, C: 7.7%, and Si: 15.9%. Figure 2(c,d)

shows high resolution XPS data taken by scanning over the W4f and O1s peaks. Four distinct peaks are again observed, but in this case the two high BE states are much larger than their Side A counterparts. Although the BE's are slightly different from those measured on Side A, the relative peak areas and the 5/2-7/2 spin-orbit doublet energy separation support the conclusion that the signals again originate from W metal and WO_3. A four-component deconvolution (Fig. 4(e)) of W4f shows that four Gaussian components are successful in modeling the peak shape, with component areas indicating that 22% of the total W4f signal originates from W metal and 78% originates from WO_3. The O1s feature from Side B (Fig. 4(d)) contains a complex structure which is similar to the O1s structure on Side A, but with growth of the high BE component at 532.0 eV. Deconvolution of O1s into two states is shown in Fig. 4(f). It is clear that the high BE component has grown substantially from Side A to Side B. In summary, WO_3 has been formed on both sides; there is more oxygen on Side B; and more WO_3 is present on Side B.

MgF_2 on Be, EOIM-3, 04-27

Figure 5(a) shows the AES spectrum for this specimen. In addition to Mg and F, the usual signals of C, N, and O are observed. Figure 5(b) shows the XPS spectrum; nothing unusual is observed. The surface stoichiometry (atomic %) determined by XPS from relative elemental sensitivity factors is: Mg: 23.2%, F: 39.6%, O: 17.1%, C: 20.1%. Figure 5(c) shows a high resolution XPS scan over the F1s peak. The F1s peak is a singlet with a measured BE of 685.5 eV. This is equal to the value obtained from MgF_2 standards reported in the literature [7]. Based on the elemental composition and F1s BE value, we conclude that a MgF_2 film has been formed.

LiF on Be, EOIM-3, 04-39

Figure 6(a) shows the AES spectrum for this specimen. In addition to Li and F, the usual C, N, and O are observed. Figure 6(b) shows the XPS spectrum from the surface; nothing unusual is found. The surface stoichiometry (atomic %) determined by XPS from relative elemental sensitivity factors is: Li: 33.5%, F: 26.9, O: 21.5%, and C:18.1%. Figure 6(c) shows a high resolution XPS scan over the F1s peak. The peak is a singlet with a measured BE of 684.8 eV. This is equal to the value obtained from LiF standards reported in the literature [7]. Based on the elemental composition and F1s BE value, we conclude that a LiF film has been formed.

Figure 7(a) shows the AES spectrum for this specimen. Only Si and O are observed. The Si peak shapes and energies are reminiscent of SiO_2, which is not unexpected; however, we have not been able to find a standard AES spectrum of SiO from the literature for comparison purposes. The XPS system suffered an electrical failure during acquisition of photoemission data from this specimen, so we cannot report an XPS spectrum at this time. We will forward the result as soon as it is available.

References

1. D. D. Sarma and C. N. R. Rao. J. Electron Spectrosc. Relat. Phenom., 20 (1980) 25.

2. F. Garbassi, J. C. J. Bart and G. Petrini, J. Electron Spectrosc. Relat. Phenom., 22 (1981) 95.

3. Y. Uwamino, T. Ishizuka, and H. Yamatera, J. Electron Spectrosc. Relat. Phenom., 34 (1984) 67.

4. R. J. Colton and J. W. Rabalais, Inorg. Chem., 15 (1976) 236.

5. G. E. McGuire, G. K. Schweitzer, and T. A. Carlson, Inorg. Chem., 12 (1973) 2450.

6. T. H. Fleisch and G. J. Mains, J. Chem. Phys. 76 (1982) 780.

7. C. D. Wagner, W. M. Riggs, L. E. Davis, J. F. Moulder, and G. E. Muilenberg, *Handbook of X-ray Photoelectron Spectroscopy* (Eden Prairie, Perkin-Elmer, 1976).

Appendix A

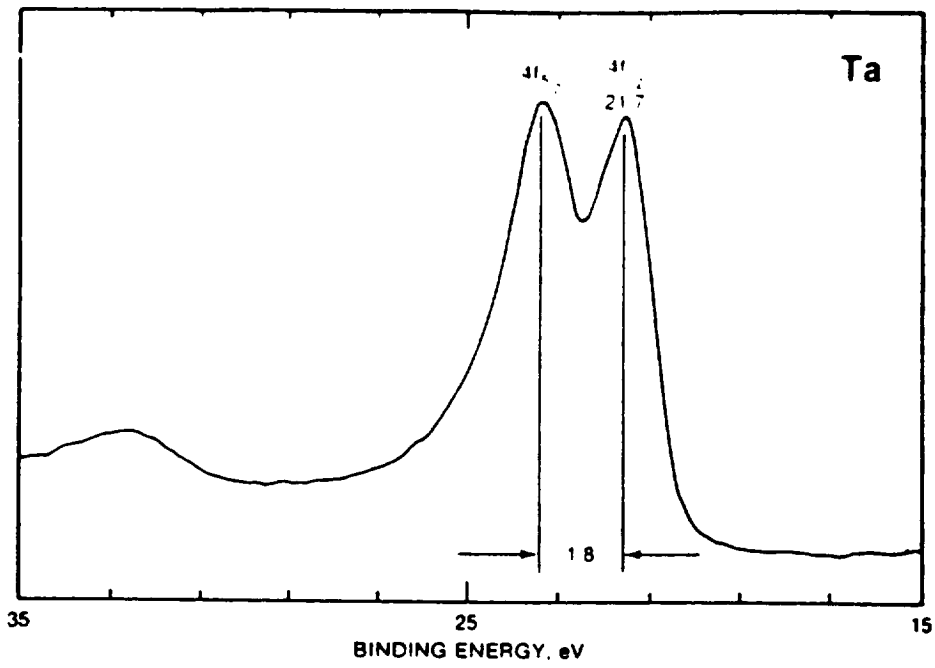

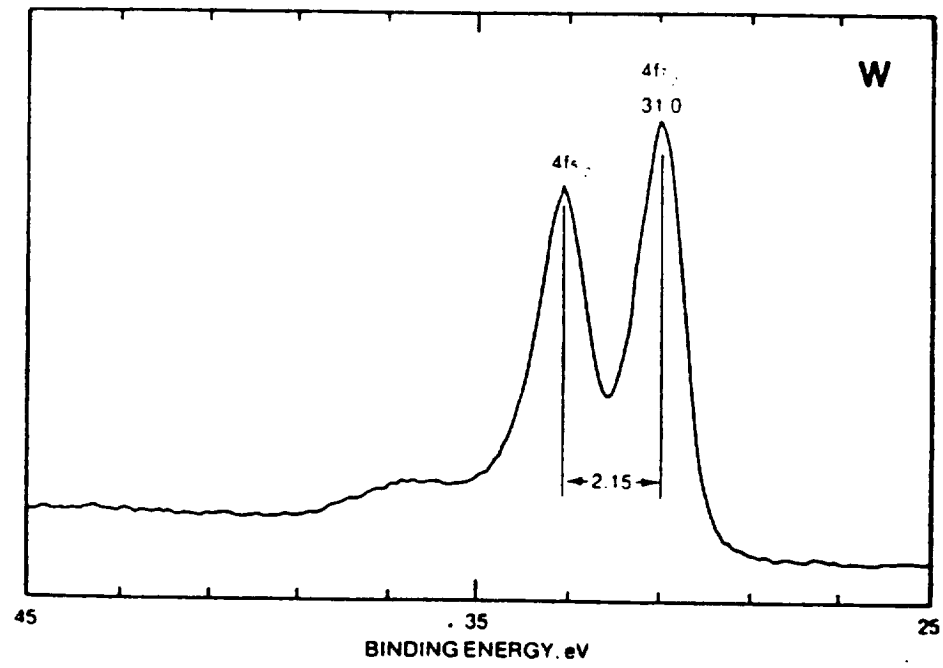

Ta and W 4f Peak Shapes Obtained from a Ta and W Metal Standard (from Ref. 7)

Appendix B

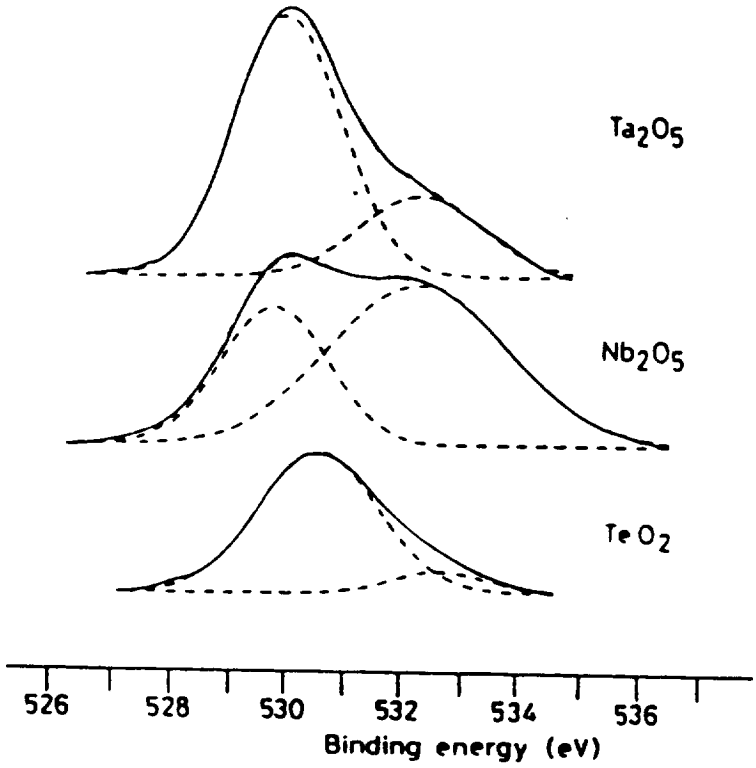

O1s Peak Shape Obtained from a Ta_2O_5 Standard Specimen (from Ref. 2)

(a)

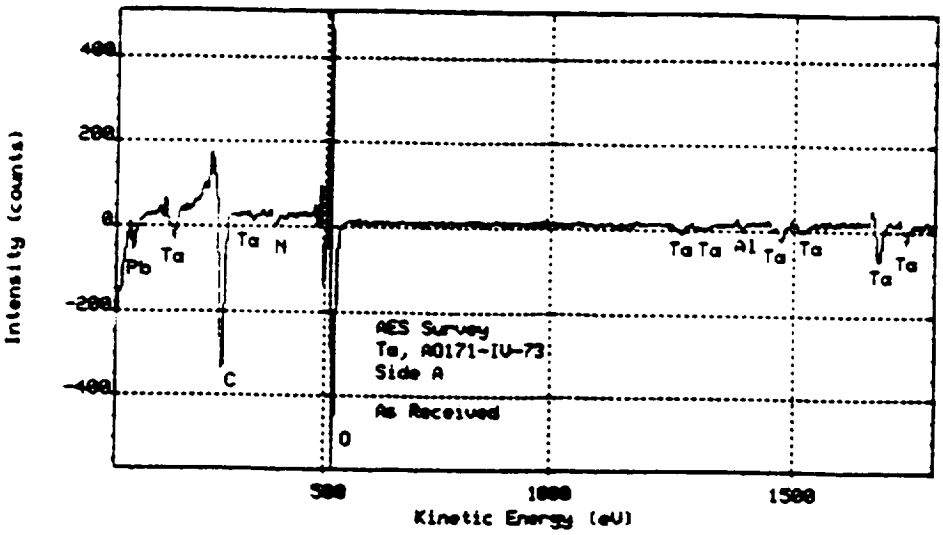

(b)

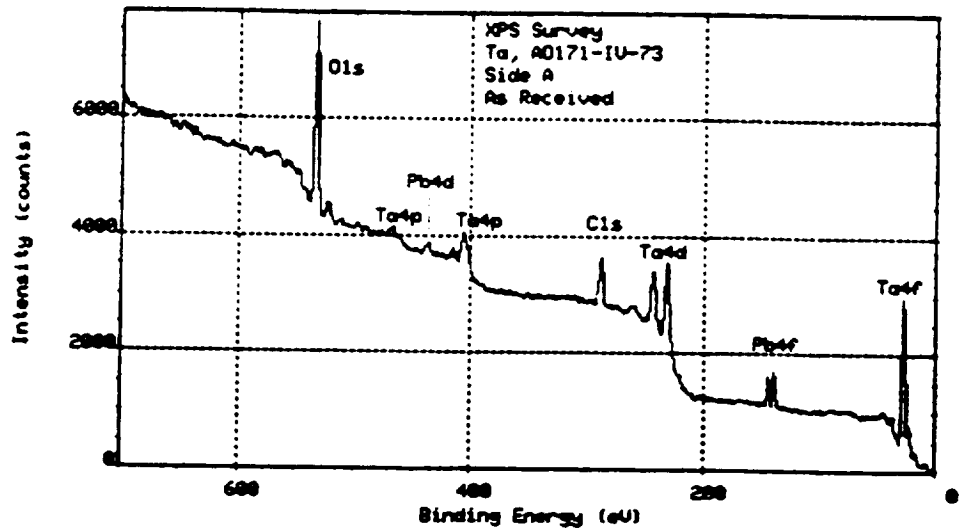

Figure 1. Ta, AO171-IV-73, Side A. (a) AES survey spectrum; (b) XPS survey spectrum.

(c)

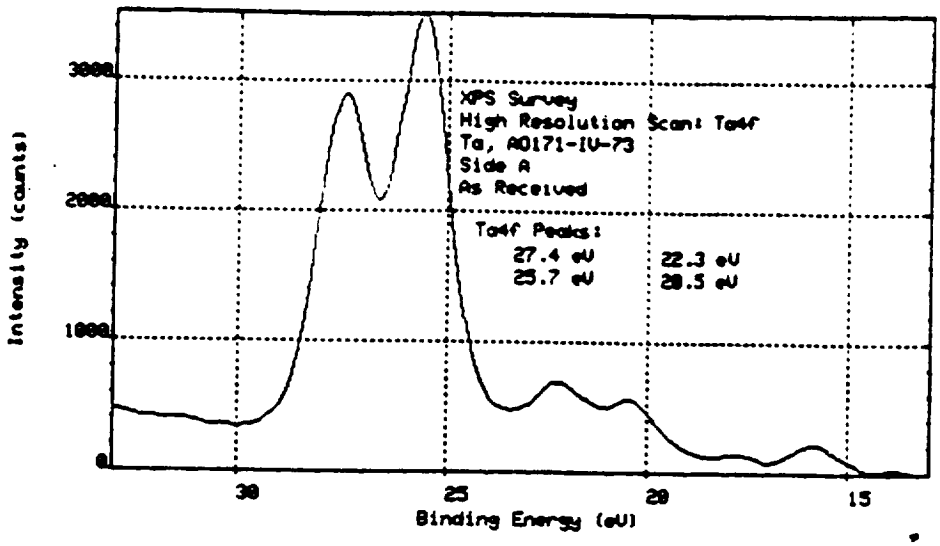

(d)

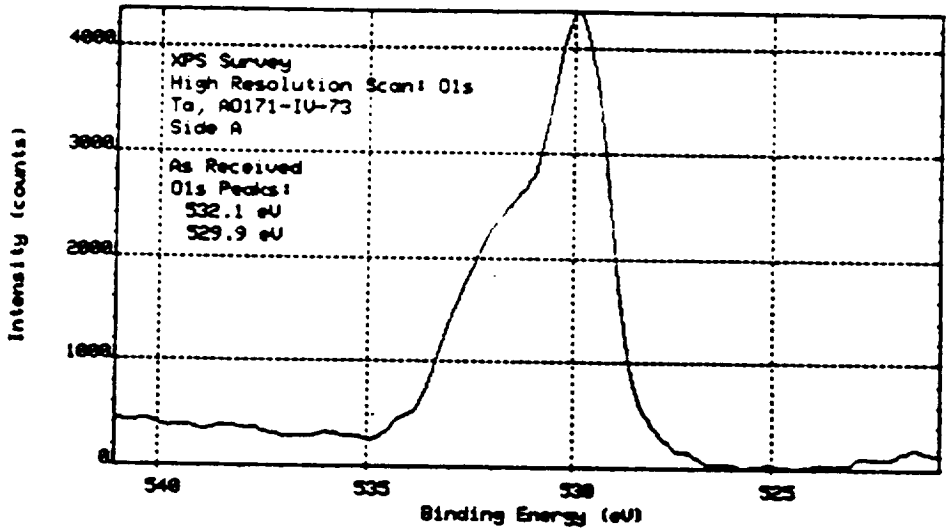

Figure 1. Ta, AO171-IV-73, Side A. (c) High resolution XPS scan over Ta4f region; (d) High resolution XPS scan over O1s region.

(e)

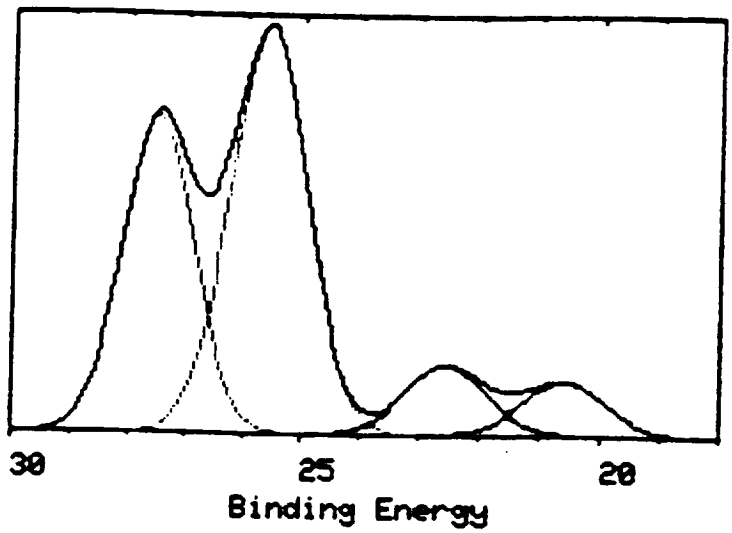

(f)

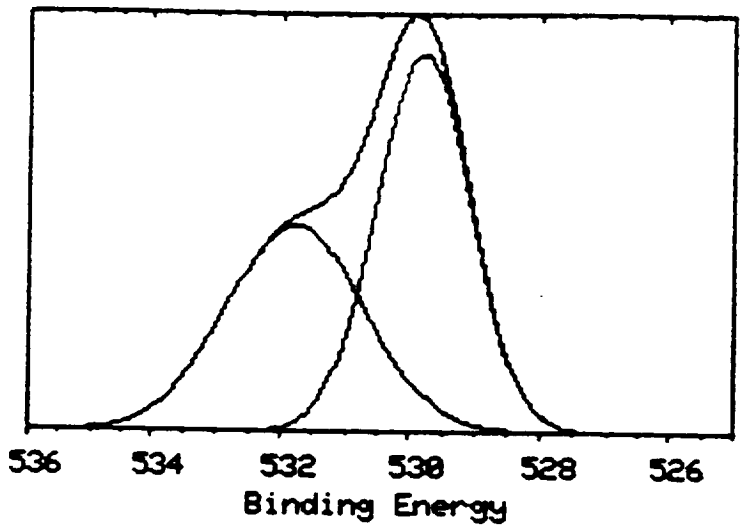

Figure 1. Ta, AO171-IV-73, Side A. (e) Deconvolution of Ta4f region using 4 components; (f) Deconvolution of O1s region using 2 components.

(a)

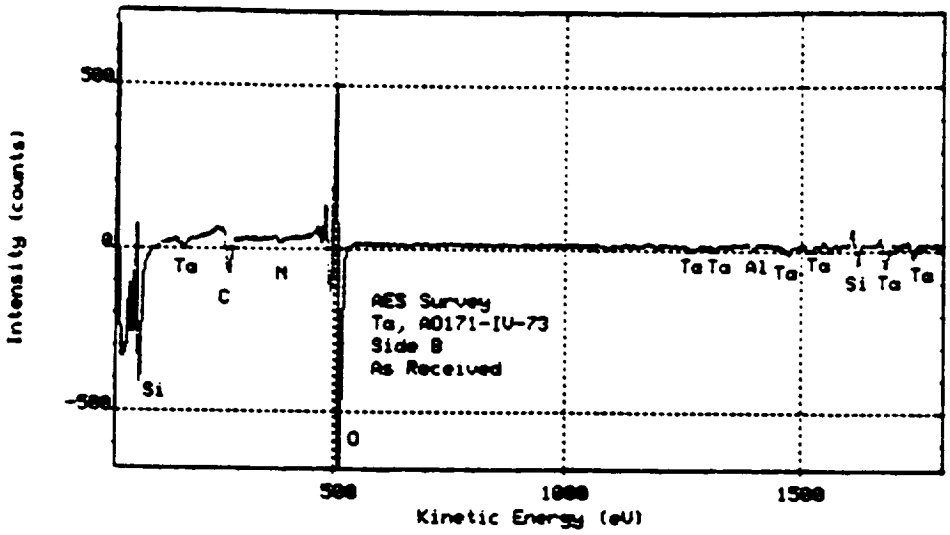

(b)

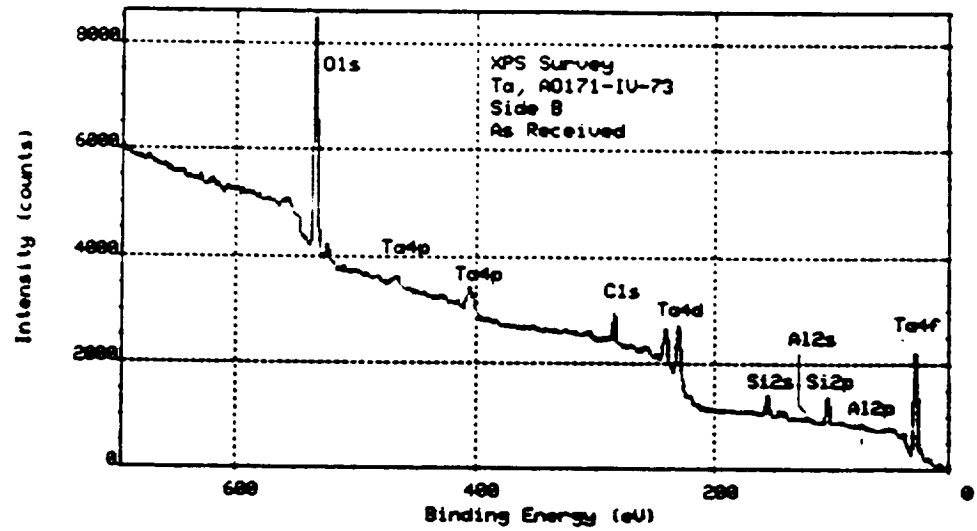

Figure 2. Ta, AO171-IV-73, Side B. (a) AES survey spectrum; (b) XPS survey spectrum.

(c)

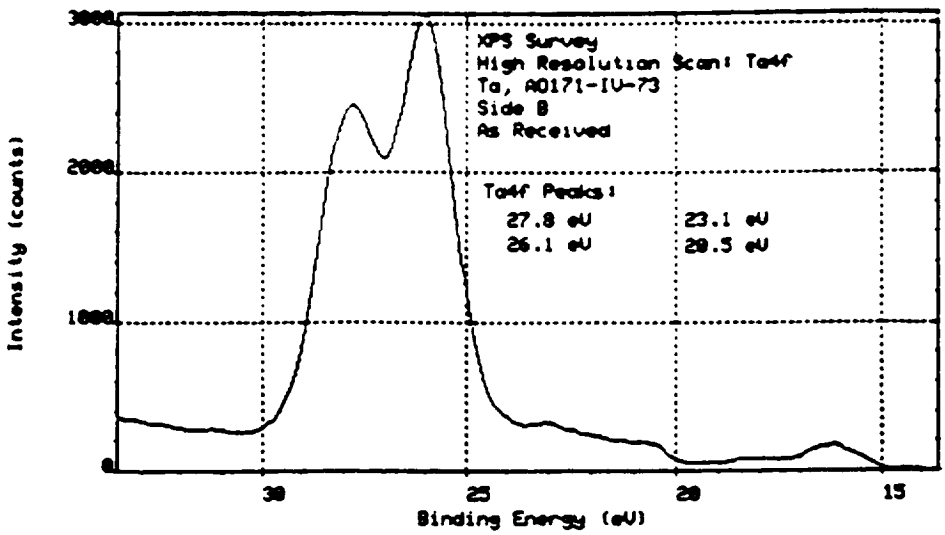

(d)

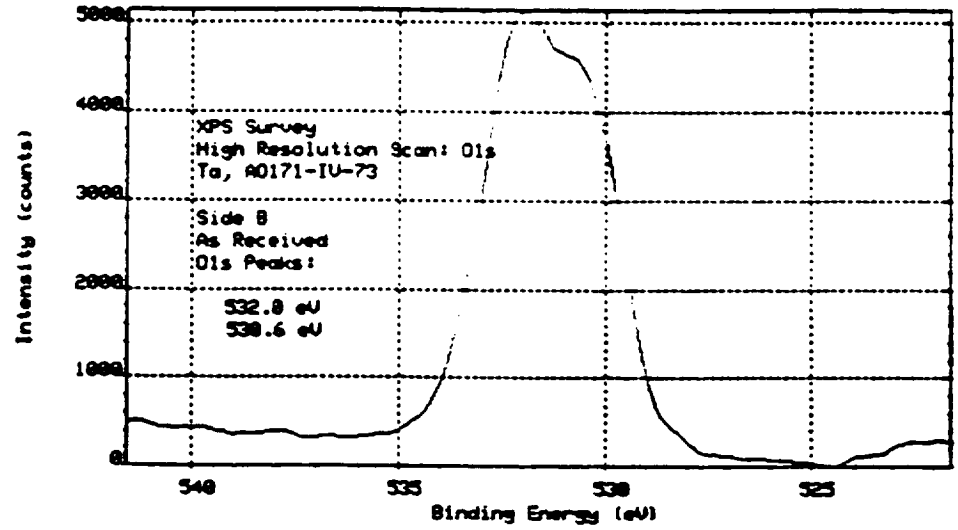

Figure 2. Ta, AO171-IV-73, Side B. (c) High resolution XPS scan over Ta4f region; (d) High resolution XPS scan over O1s region.

(e)

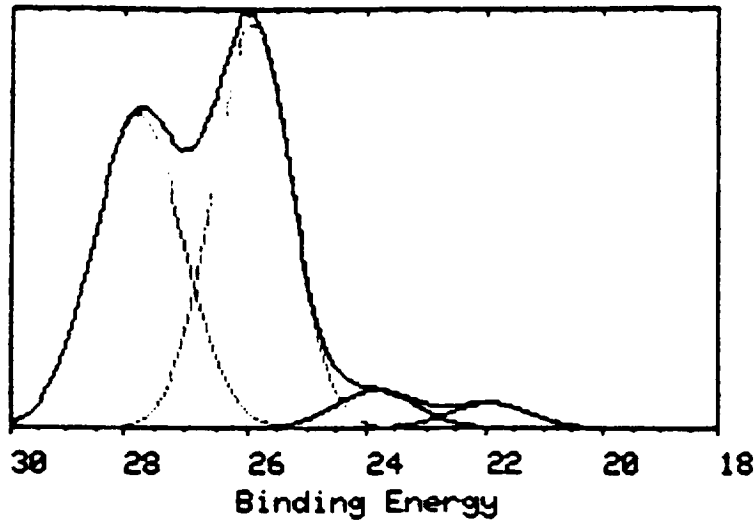

(f)

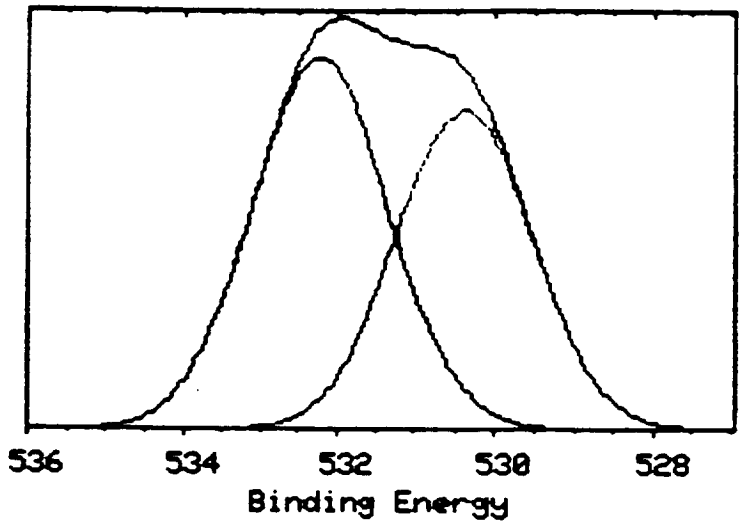

Figure 2. Ta, AO171-IV-73, Side B. (e) Deconvolution of Ta4f region using 4 components; (f) Deconvolution of O1s region using 2 components.

(a)

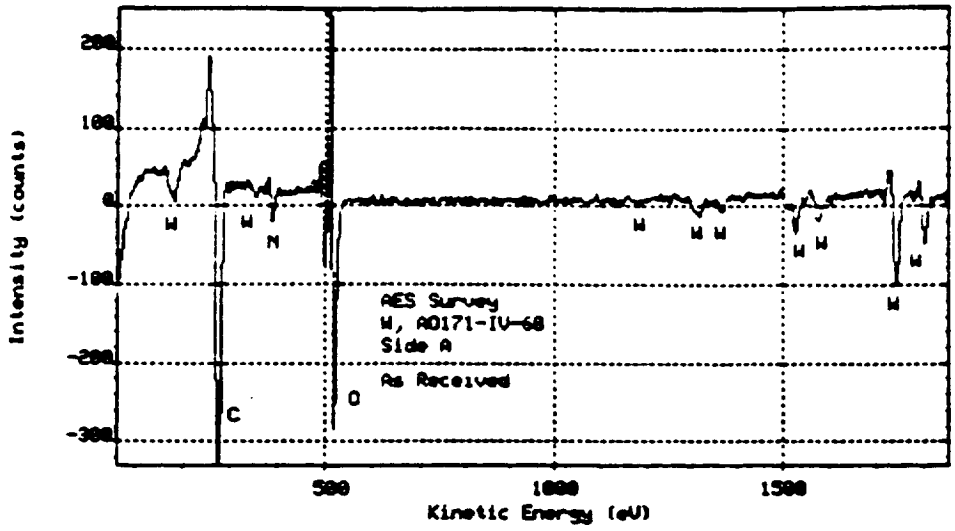

(b)

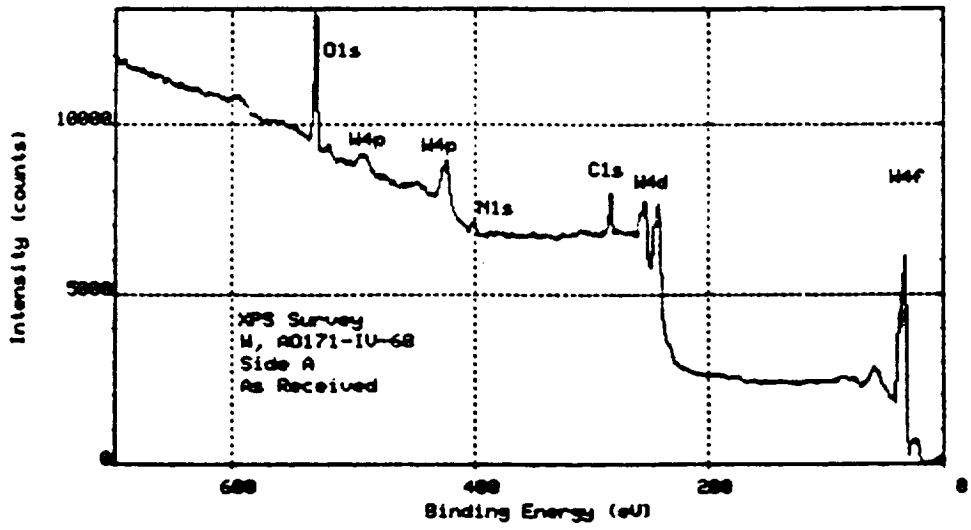

Figure 3. W, AO171-IV-68, Side A. (a) AES survey spectrum; (b) XPS survey spectrum.

(c)

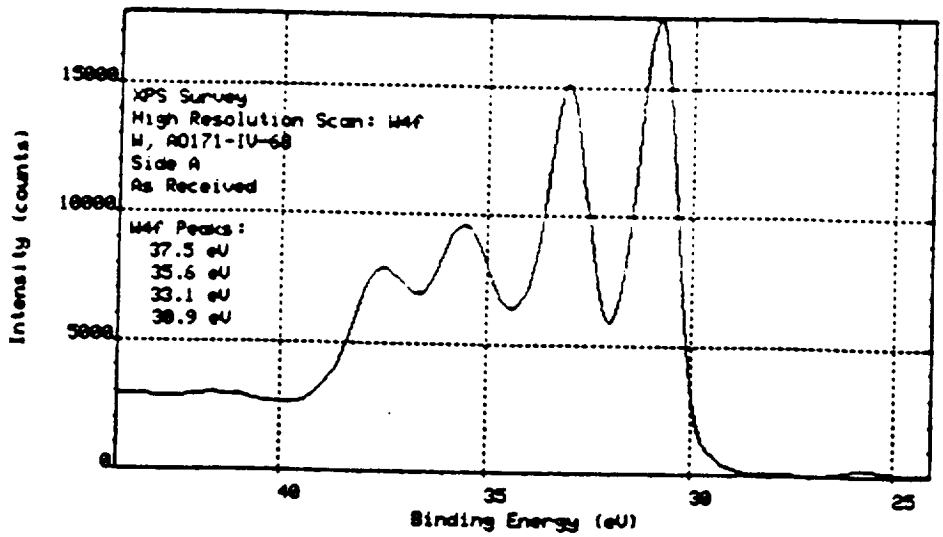

(d)

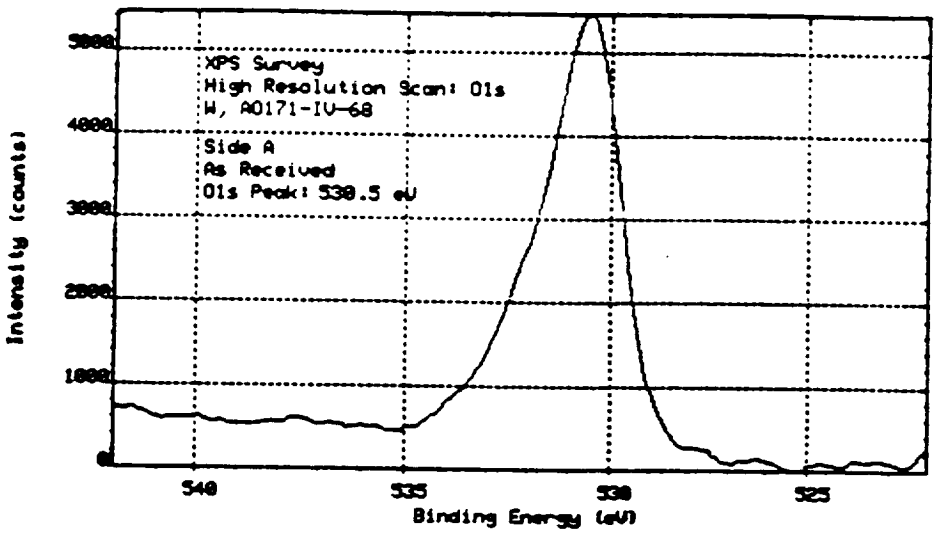

Figure 3. W, AO171-IV-68, Side A. (c) High resolution XPS scan over W4f region; (d) High resolution XPS scan over O1s region.

(e)

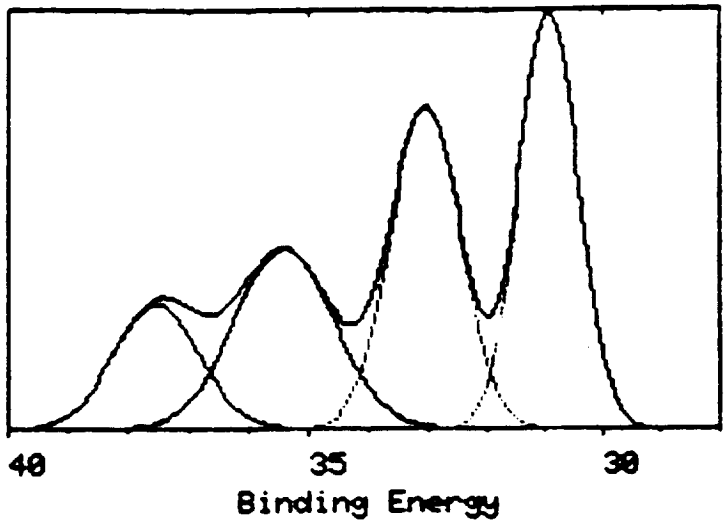

(f)

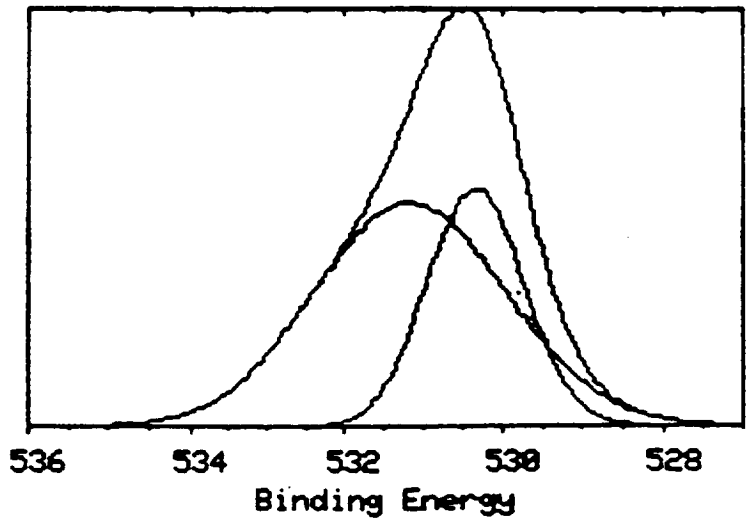

Figure 3. W, AO171-IV-68, Side A. (e) Deconvolution of W4f region using 4 components; (f) Deconvolution of O1s region using 2 components.

(a)

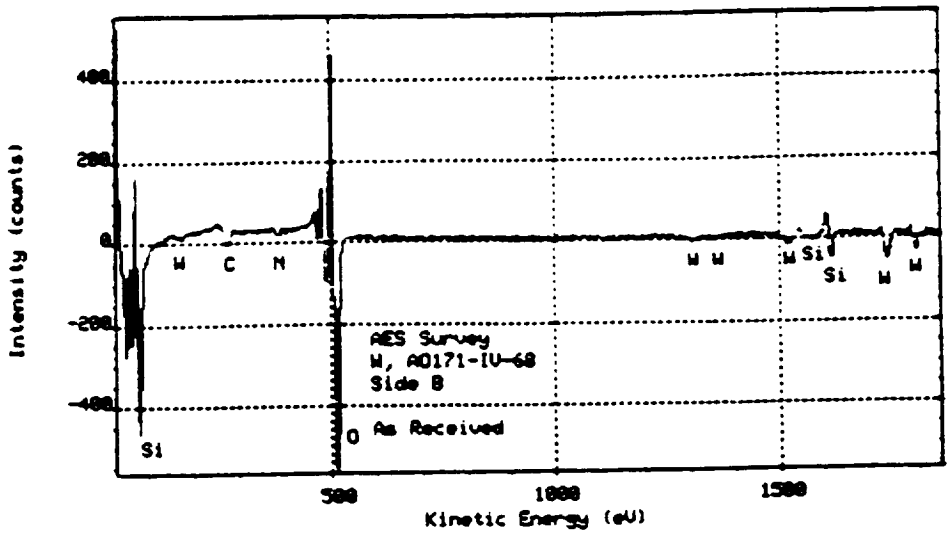

(b)

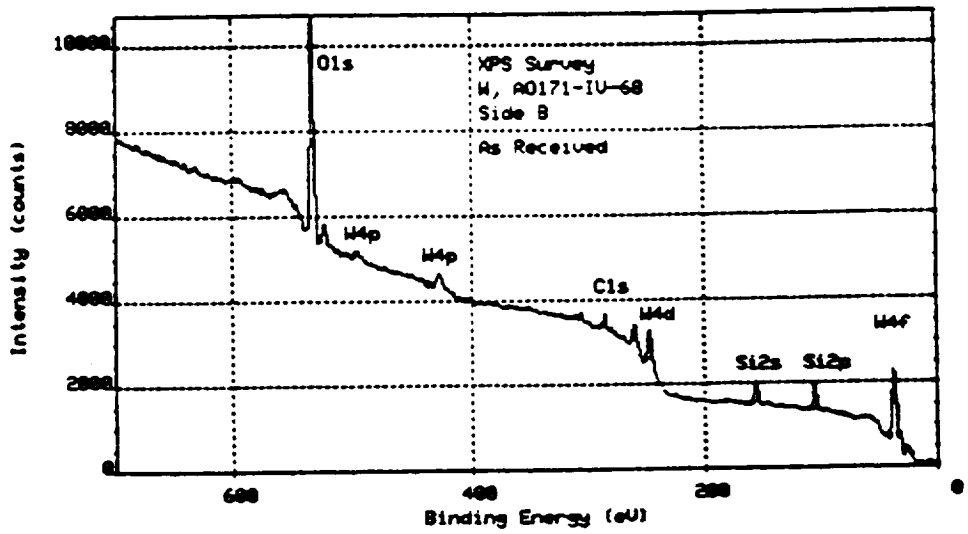

Figure 4. W, AO171-IV-68, Side B. (a) AES survey spectrum; (b) XPS survey spectrum.

(c)

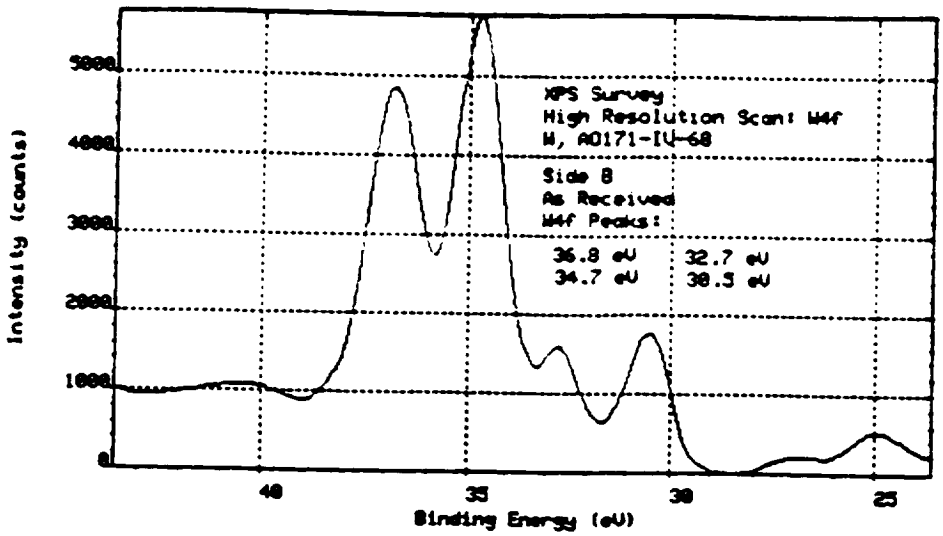

(d)

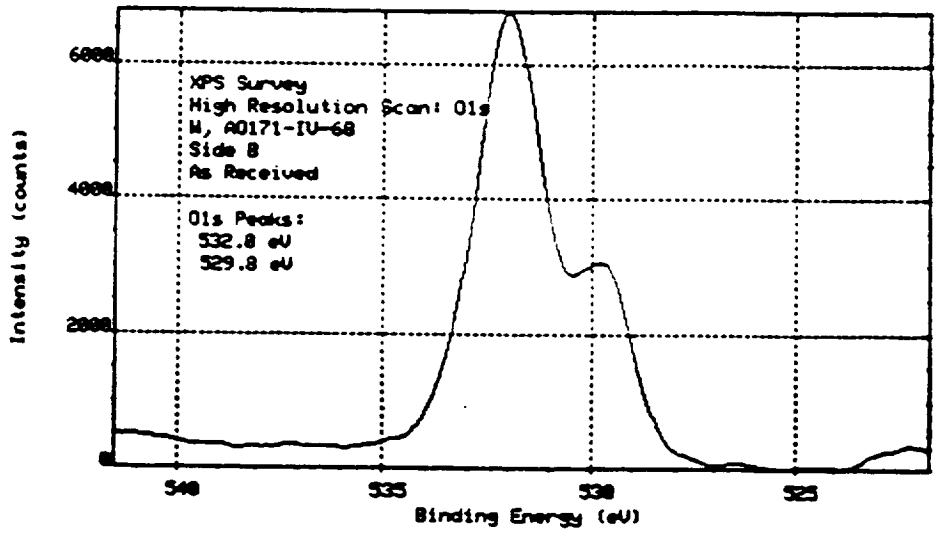

Figure 4. W, AO171-IV-68, Side B. (c) High resolution XPS scan over W4f region; (d) High resolution XPS scan over O1s region.

(e)

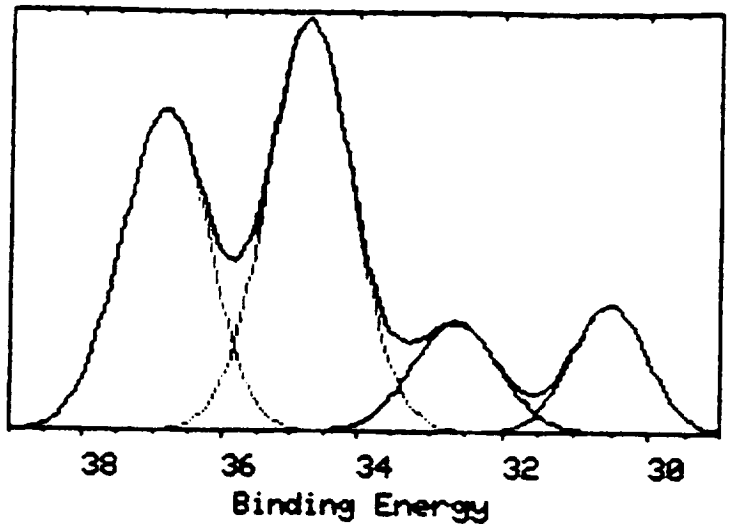

(f)

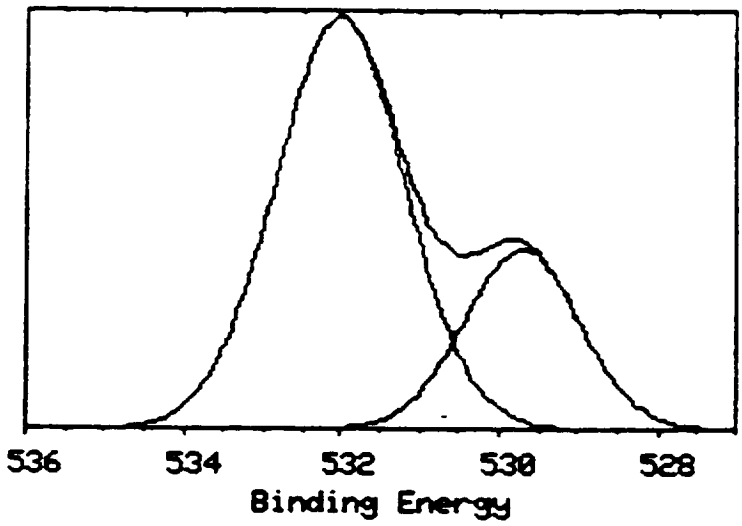

Figure 4. W, AO171-IV-68, Side B. (e) Deconvolution of W4f region using 4 components; (f) Deconvolution of O1s region using 2 components.

(a)

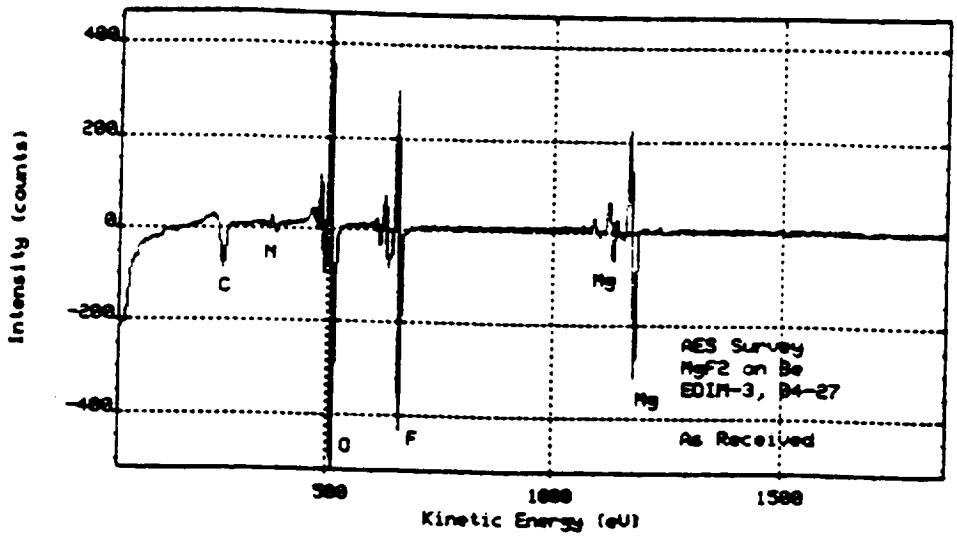

(b)

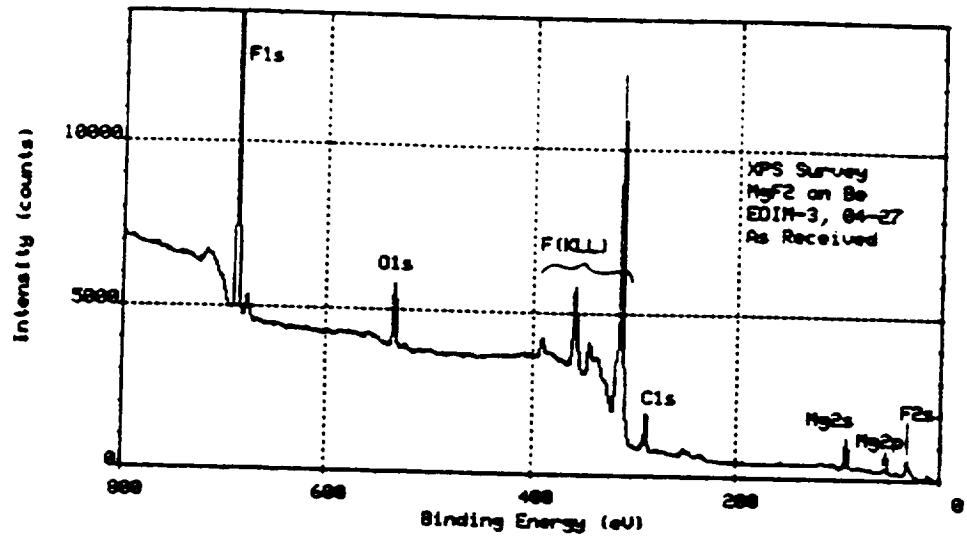

Figure 5. MgF_2 on Be, EOIM-3, 04-27. (a) AES survey spectrum; (b) XPS survey spectrum.

(c)

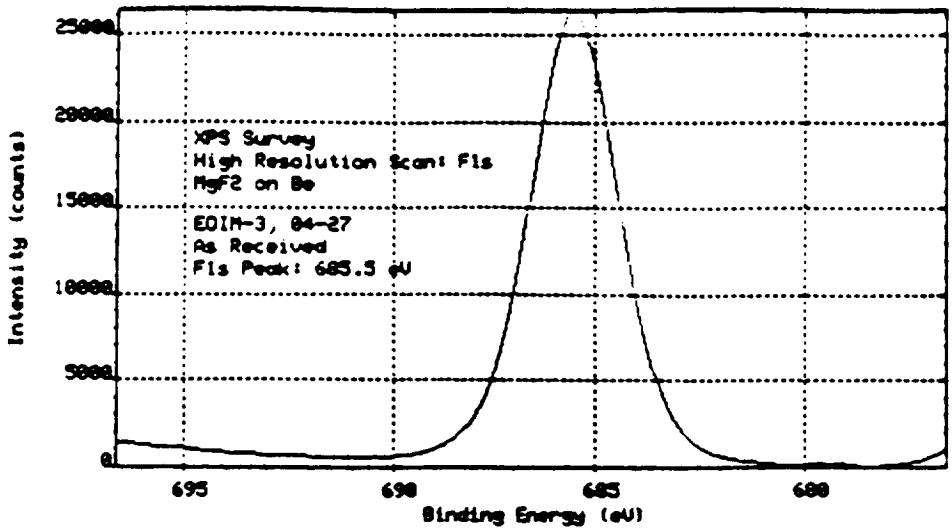

Figure 5. MgF_2 on Be, EOIM-3, 04-27. (c) High resolution XPS scan over F1s region.

(a)

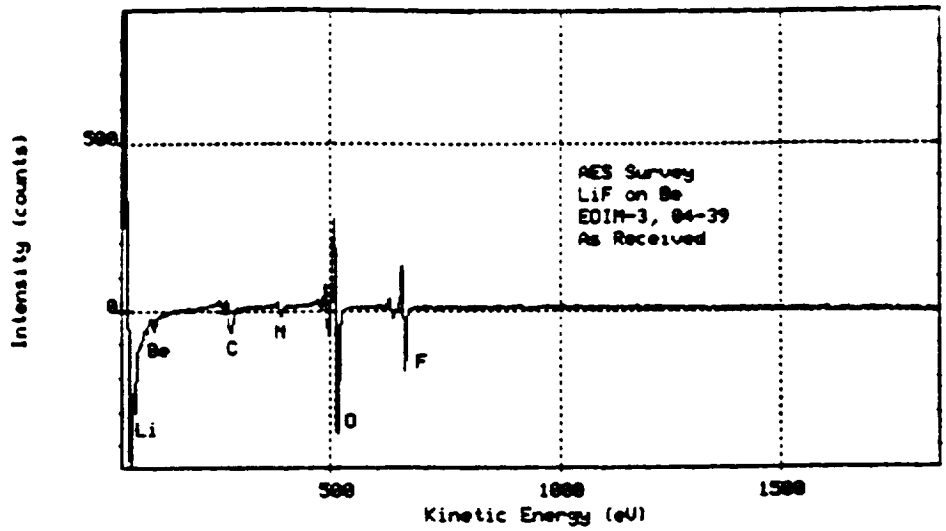

(b)

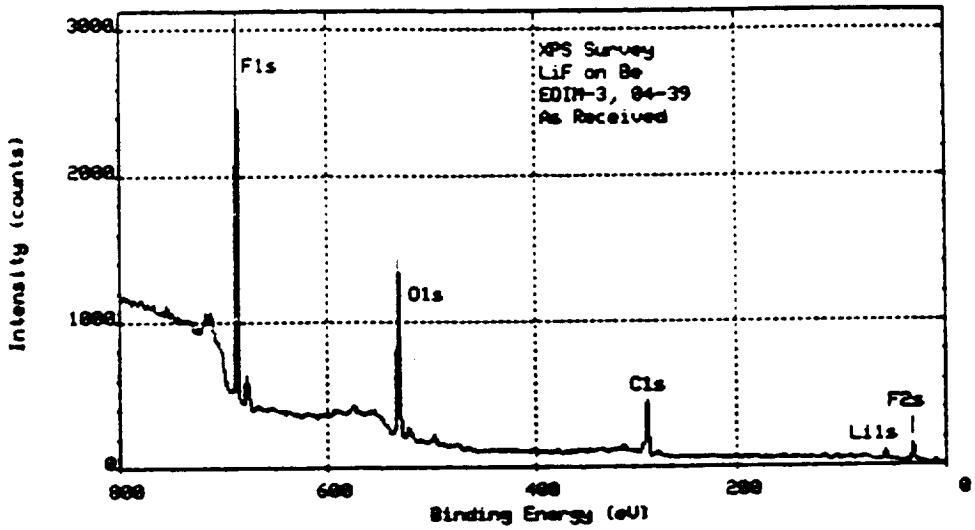

Figure 6. LiF on Be, EOIM-3, 04-39. (a) AES survey spectrum; (b) XPS survey spectrum.

(c)

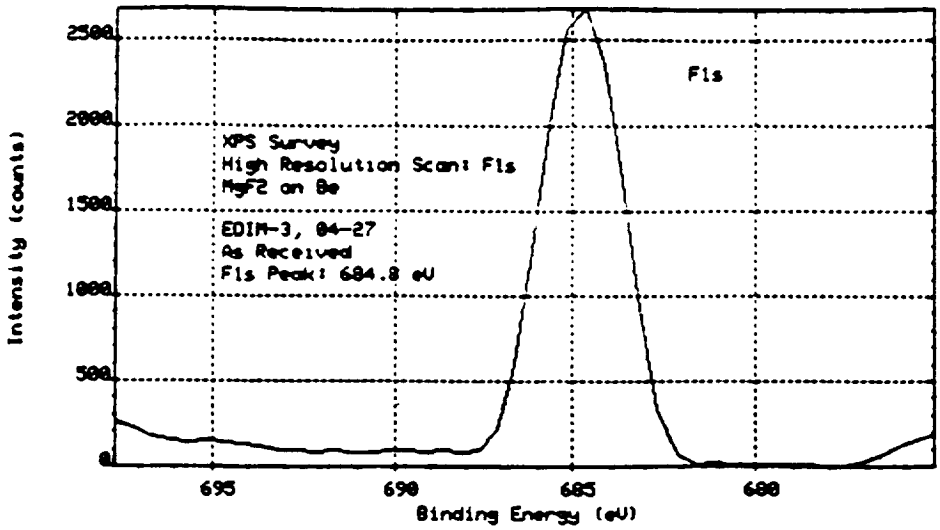

Figure 6. LiF on Be, EOIM-3, 04-27. (c) High resolution XPS scan over F1s region.

Rutherford Back Scattering

1. Introduction

Ten RBS spectra have been acquired and analyzed for the following MSFC samples: AO171-1V-68, AO171-1V-73, EO1M-3-04-27, EO1M-3-04-38 and EO1M-3-04-39. For each sample, two spectra were generated - one for an "unexposed" region of the sample and one for an "exposed" region as shown in the following diagram.

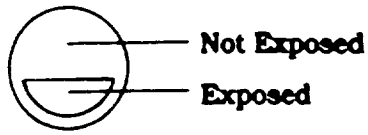

A 2 MeV, 7 nA He^+ particle beam was used to generate the RBS spectra. The beam was incident along the surface normal of each sample, and scattered alpha particles were detected with a silicon surface barrier detector positioned at 170^0 with resoect to the incident beam direction. This detector subtends a solid angle of 7.4 mstr.

Two addirional simulations have been included for the unexposed spectrum of sample AO171-1V-73 (Figs. 3 and 4.) for the purpose of discussing the sensitivity of the RBS measurements for this sample. Altogether, twelve spectra are presented - eight with simulations and four without.

2. Results

Samples AO171-1V-69 (Pure Tungsten) and AO171-1V-73 (Pure Tantalum)

RBS spectra for these samples are shown in Figures 1 and 2. The normalized yields are different for the unexposed and exposed spectra for each sample because the unexposed portion of each sample was irradiated for a slightly longer time. As can be seen, the RBS technique shows essentially no difference between the two regions (exposed and unexposed) on both samples. Figures 3 and 4 indicate why this may be true. These figures show simulations for the unexposed spectrum of sample 1V-73 assuming no Ta_2O_5 layer on the Ta surface (Fig. 3) and 50nm of Ta_2O_5 on the Ta surface (Fig. 4). For thin film surface layers of a heavy metal oxide on a thick heavy metal substrate, the RBS technigue does not provide the necessary sensitivity for a truly accurate analysis of the sample surface.

Sample EO1M-3-04-27 (Figures 5 and 6)

The solid curves in Figures 5 and 6 represent simulations of the measured spectra generated using the computer code RUMP. The same layer structure was used for both regions of the sample, indicating no dramatic change for the exposed region compared to the unexposed region. Zinc and Mn appear to be present in the Be substrate with some Mn and Zn having moved foward to the surface of the MgF_2 layer for both the unexposed and exposed regions. Heating, rather exposure to atomic oxygen, could cause this. Additionally for both regions, O appears in the MgF_2 layer and in the surface region of the Be substrate. The high, narrow peak near channel 450 in each spectrum may result from a thin layer of some metal heavier than Ta which is positioned between the MgF_2 layer and the Be substrate. However, the data in Figures 5 and 6 are well simulated assuming a thin Ta surface layer.

Sample EO1M-3-04-38 (Figures 7 and 8)

The exposed and unexposed regions of this sample do not appear significantly different. Both spectra can be simulated with a 150 nm layer of SiO_2 on a thick Be substrate. The Be substrate appears to contain Zn.

Sample EO1M-3-04-39 (Figures 9 and 10)

Again, exposure does not appear to have significantly affected this sample which consists of a thin LiF layer on a thick Be substrate. Zinc, Mn and O are present in the LiF layer and in the surface region of the substrate. However, since these three elements appear for both the exposed and unexposed regions, their presence may not have been caused solely by exposure to atomic oxygen.

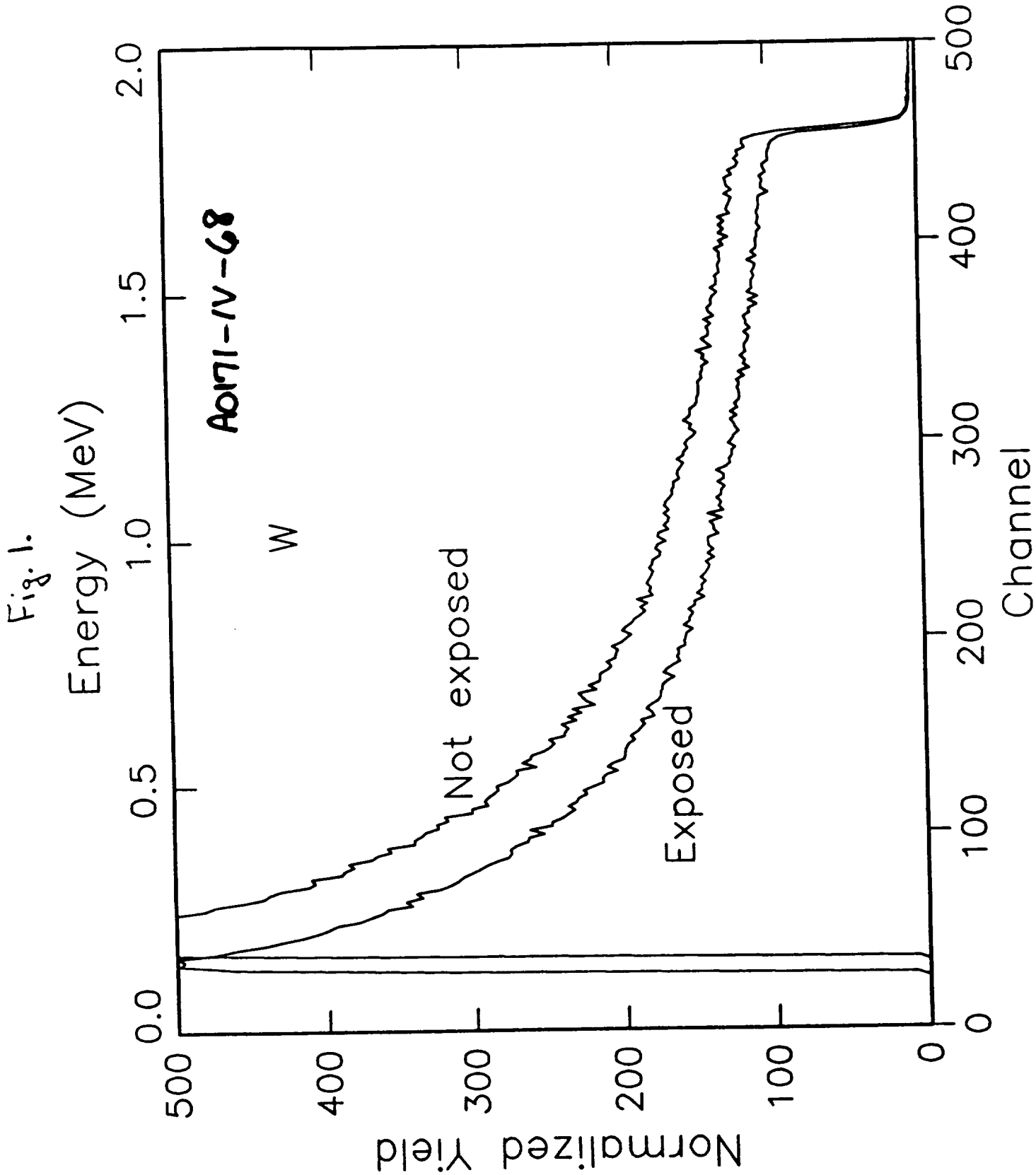
Fig. 1.
Energy (MeV)
0.0
0.5
1.0
1.5
2.0
W
A0171-IV-68
Not exposed
Exposed
Normalized Yield
500
400
300
200
100
0
Channel
0
100
200
300
400
500

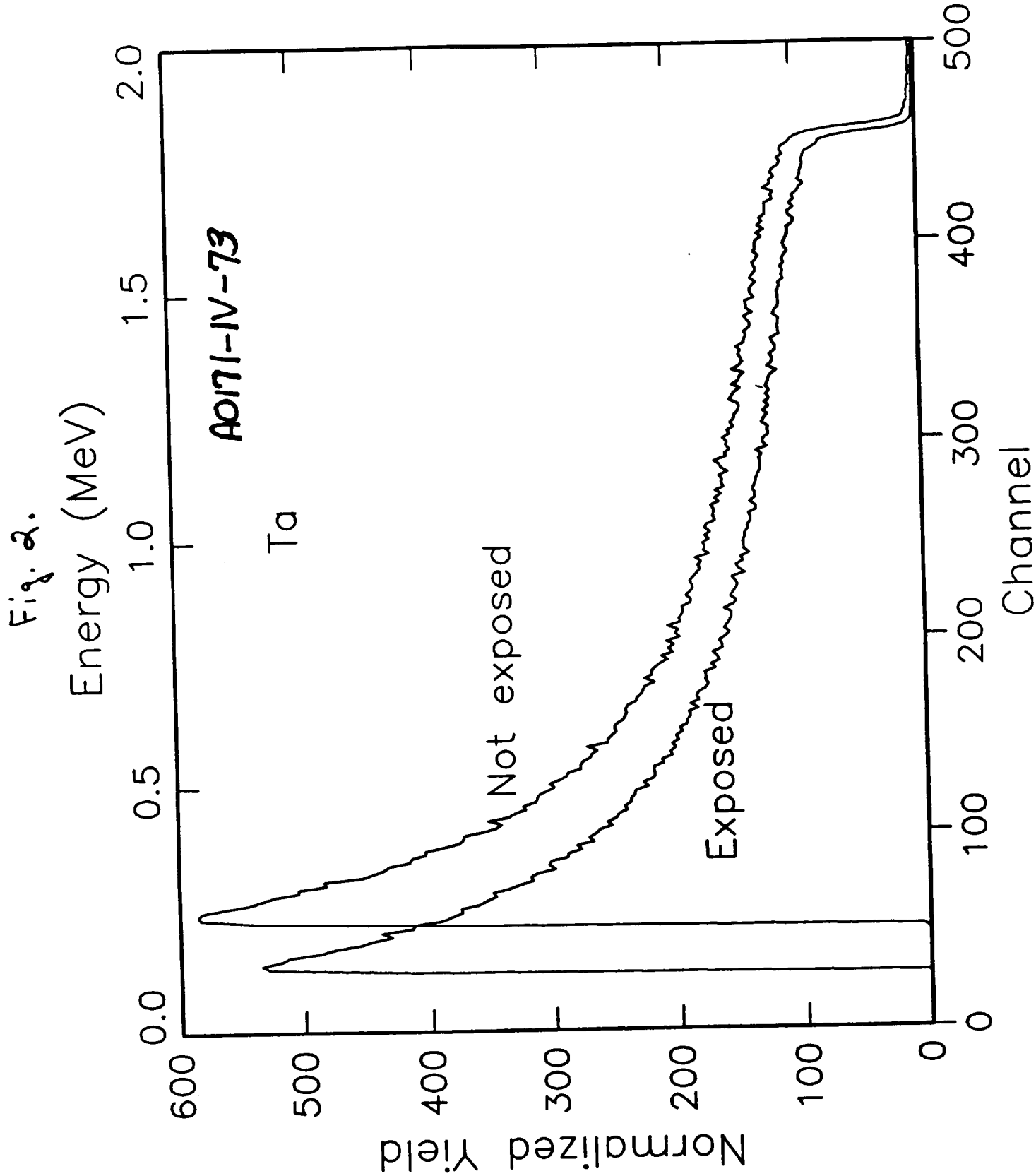
Fig. 2.
Energy (MeV)
0.0
0.5
1.0
1.5
2.0
AON1-IV-73
Ta
Not exposed
Exposed
Normalized Yield
600
500
400
300
200
100
0
Channel
0
100
200
300
400
500

Fig. 3.

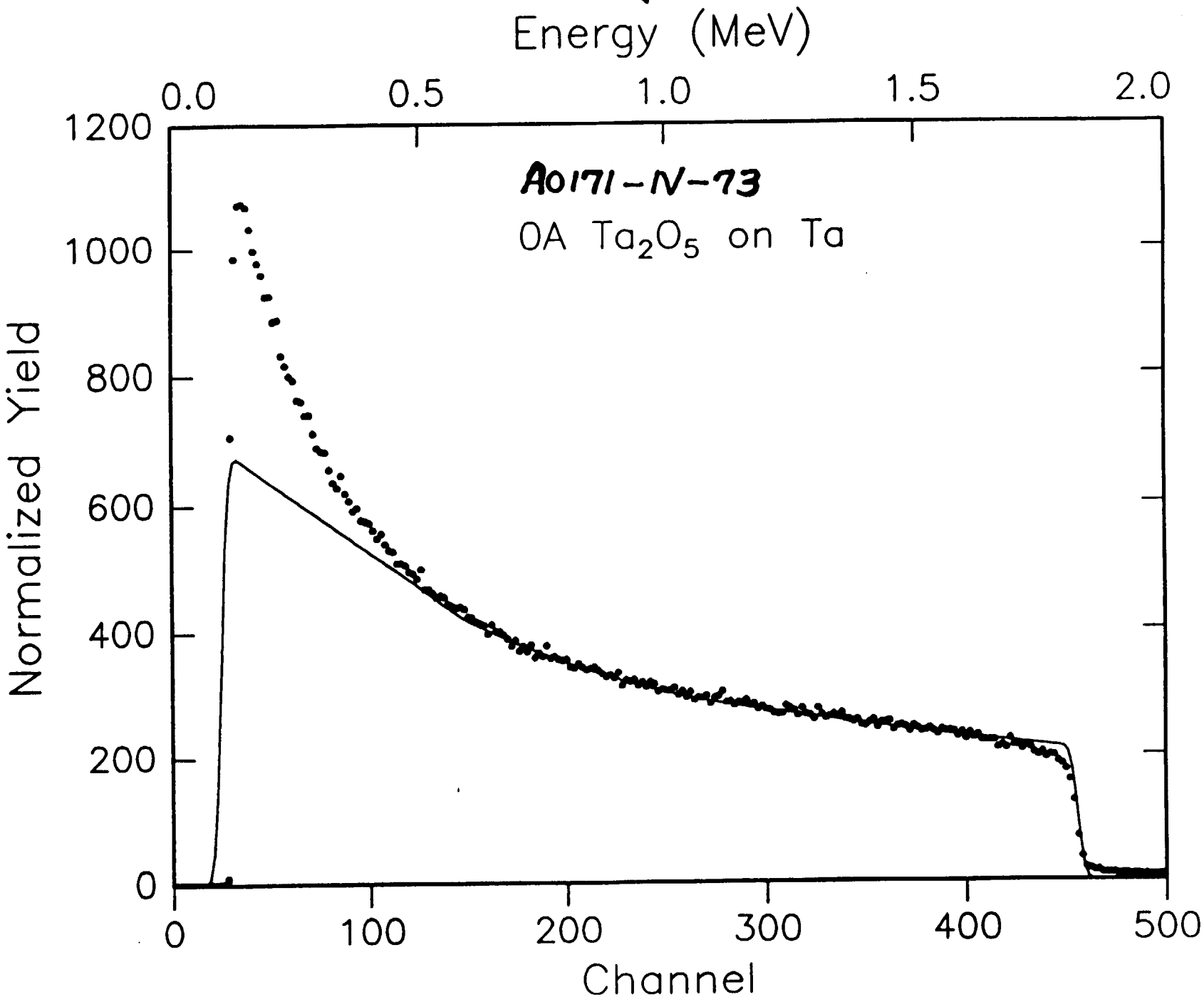
Energy (MeV)
0.0
0.5
1.0
1.5
2.0
A0171-IV-73
0A Ta_2O_5 on Ta
Normalized Yield
1200
1000
800
600
400
200
0
0
100
200
300
400
500
Channel

Fig. 4.

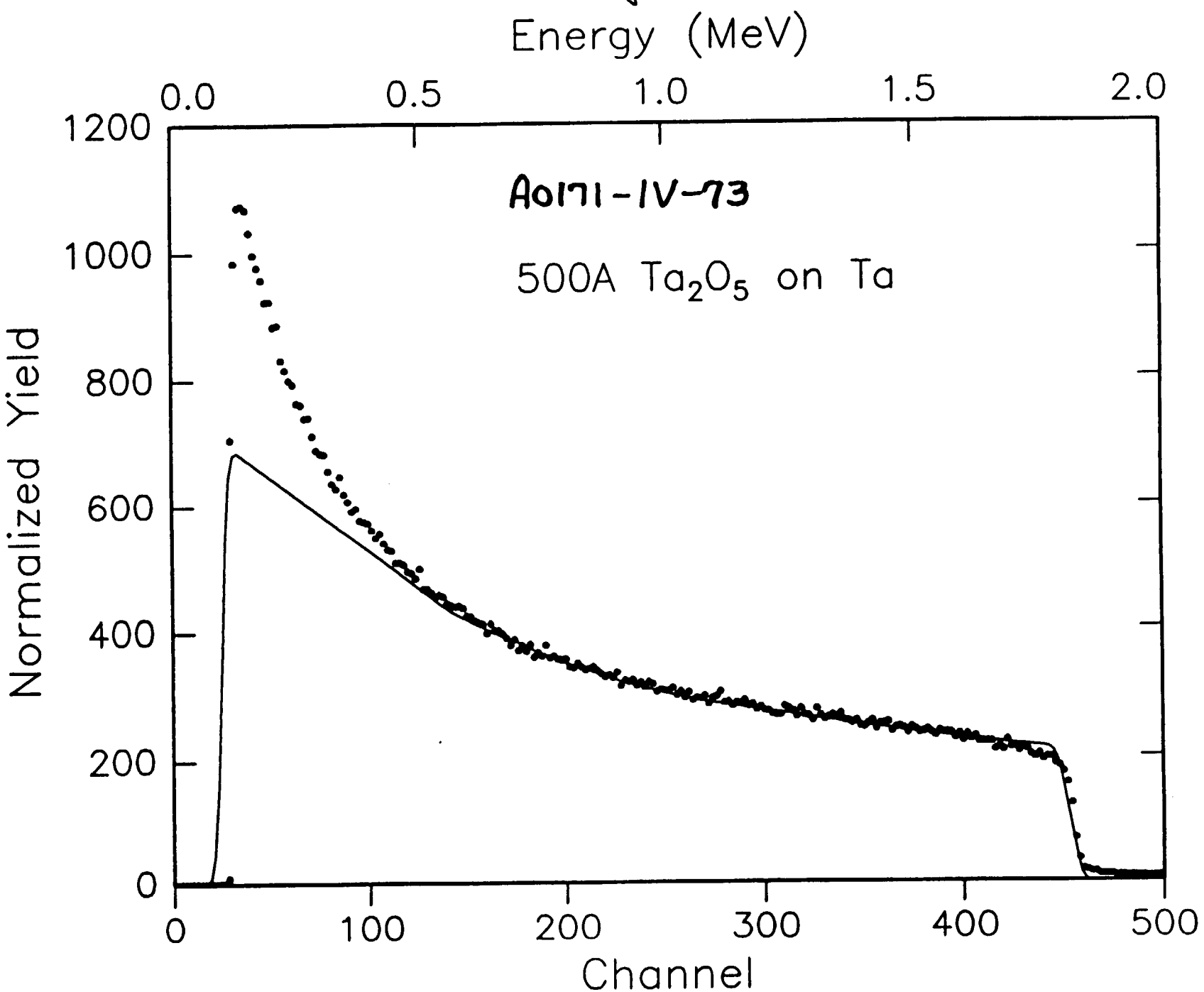
Energy (MeV)
0.0
0.5
1.0
1.5
2.0
1200
1000
800
600
400
200
0
Normalized Yield
A0171-IV-73
500A Ta_2O_5 on Ta
0
100
200
300
400
500
Channel

Fig. 5.

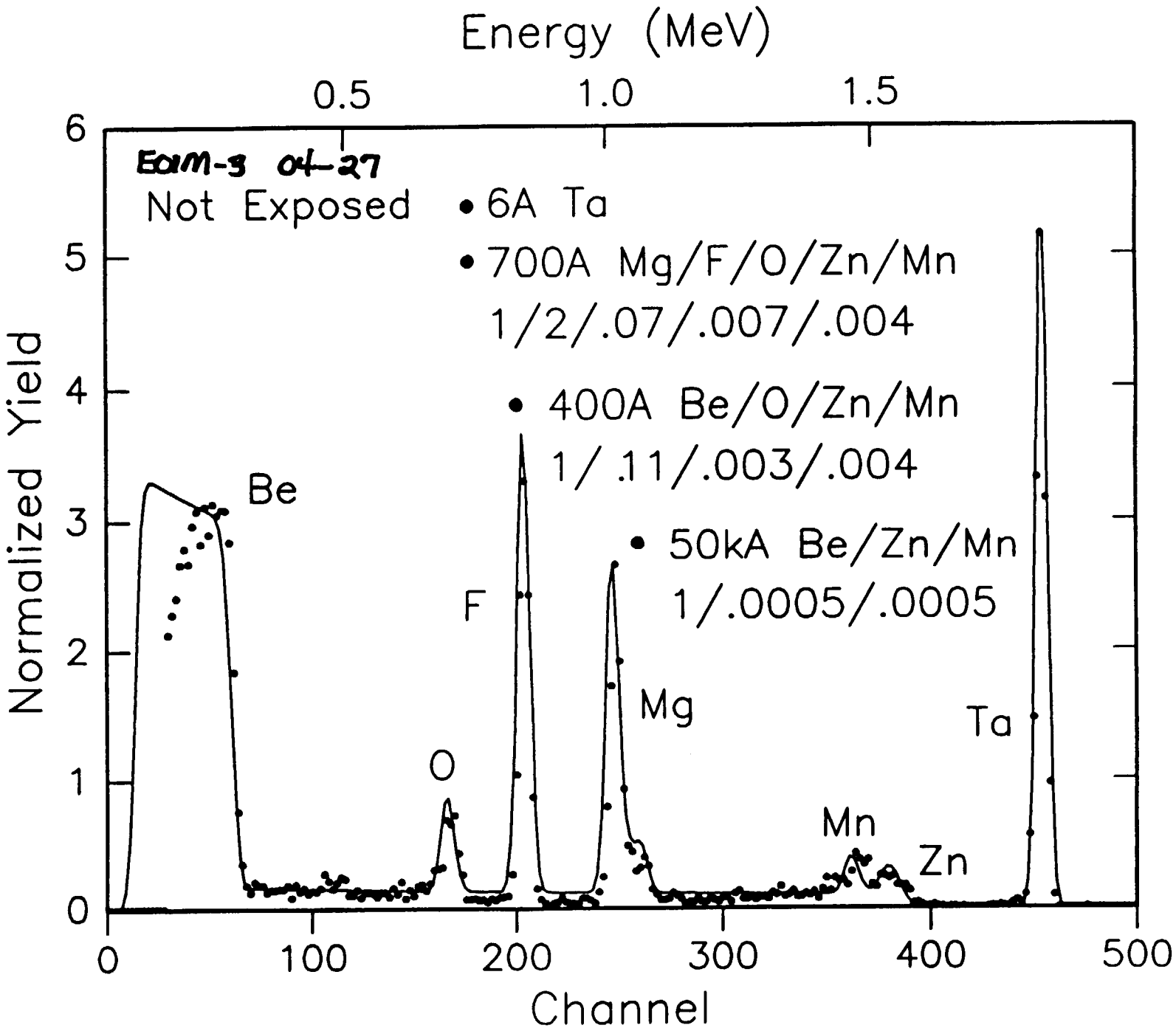
Energy (MeV)
0.5
1.0
1.5
EAM-3 04-27
Not Exposed
• 6A Ta
• 700A Mg/F/O/Zn/Mn
1/2/.07/.007/.004
• 400A Be/O/Zn/Mn
1/ .11/.003/.004
• 50kA Be/Zn/Mn
1/.0005/.0005
Normalized Yield
Be
O
F
Mg
Mn
Zn
Ta
0
1
2
3
4
5
6
0
100
200
300
400
500
Channel

Fig. 6.

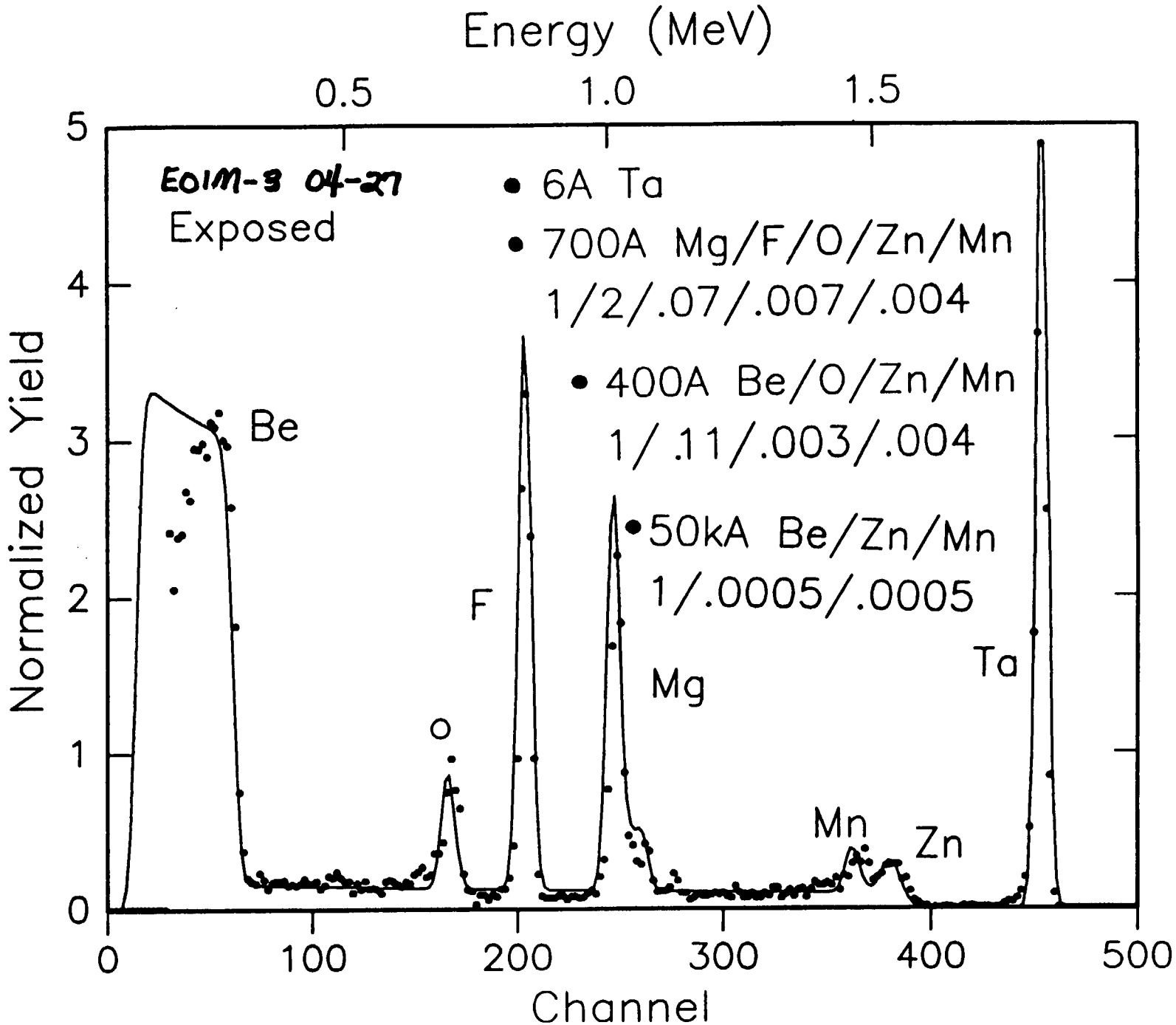
Energy (MeV)
0.5
1.0
1.5
EOIM-3 04-27
Exposed
• 6A Ta
• 700A Mg/F/O/Zn/Mn
1/2/.07/.007/.004
• 400A Be/O/Zn/Mn
1/.11/.003/.004
• 50kA Be/Zn/Mn
1/.0005/.0005
Be
O
F
Mg
Mn
Zn
Ta
Normalized Yield
0
1
2
3
4
5
0
100
200
300
400
500
Channel

Fig. 7.

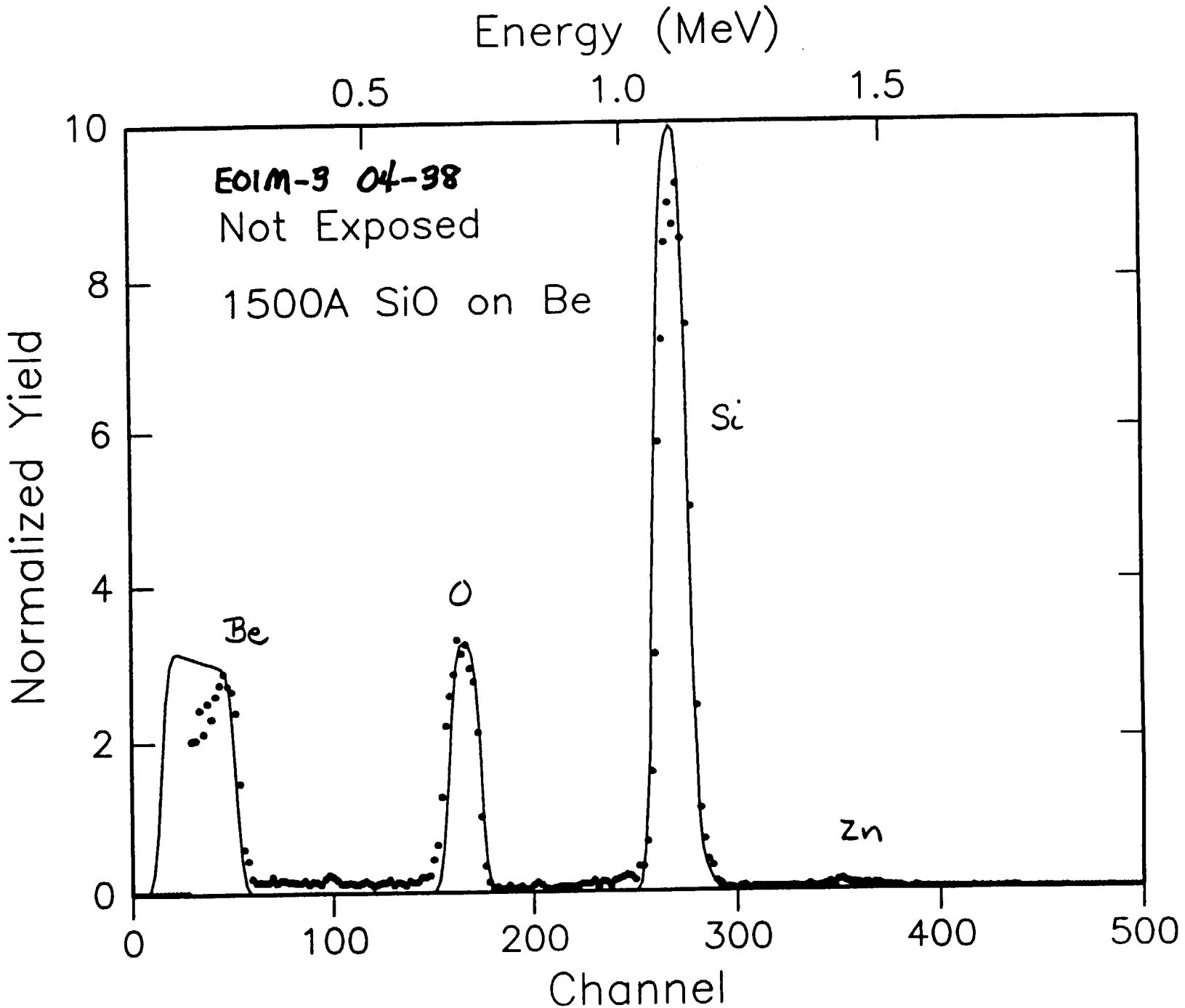
Energy (MeV)
0.5
1.0
1.5
EOIM-3 04-38
Not Exposed
1500A SiO on Be
Be
O
Si
Zn
Normalized Yield
Channel
0
2
4
6
8
10
0
100
200
300
400
500

Fig. 8.

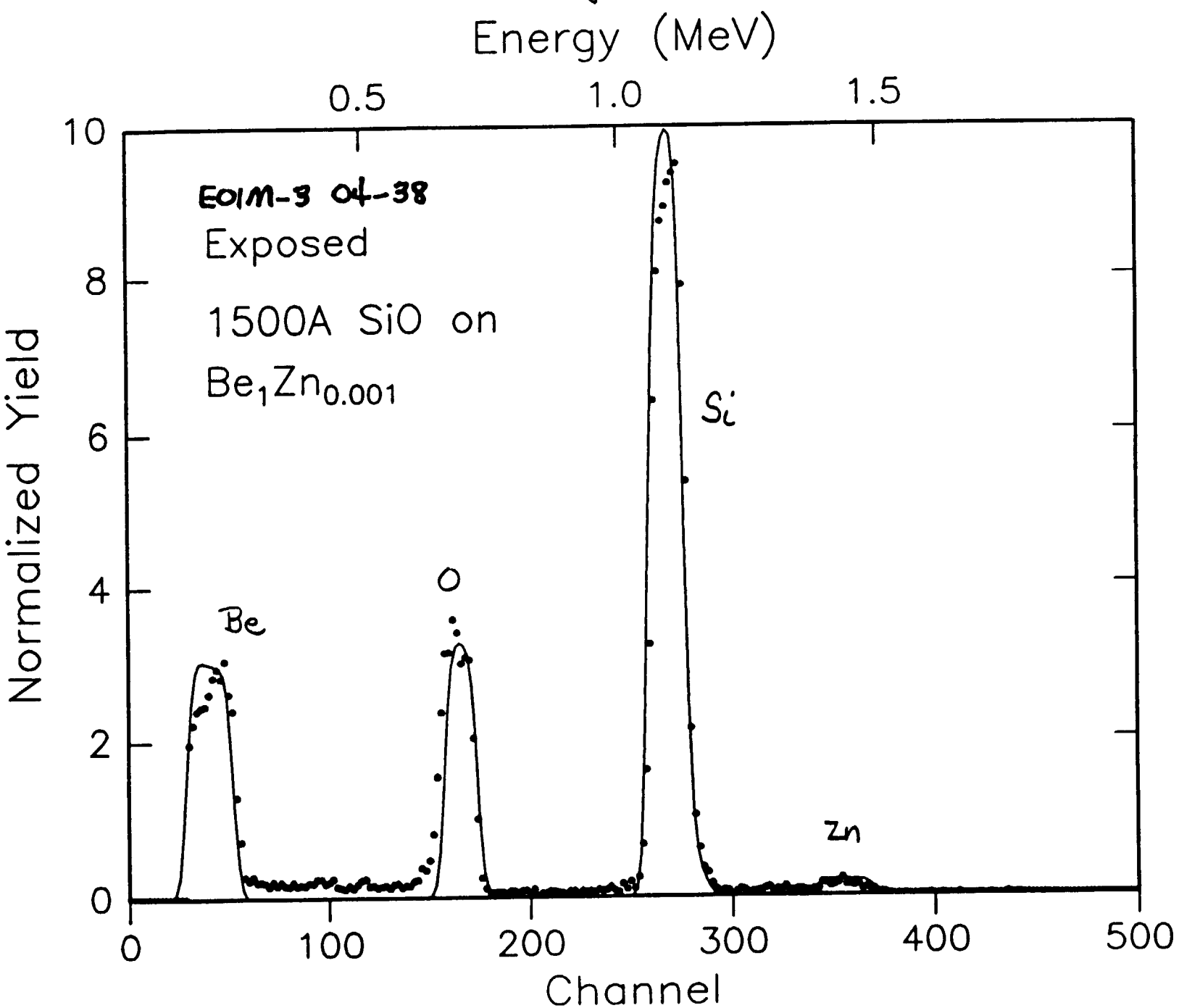
Energy (MeV)
0.5
1.0
1.5
EOIM-3 04-38
Exposed
1500A SiO on
$Be_1Zn_{0.001}$
Be
O
Si
Zn
Normalized Yield
Channel
0
2
4
6
8
10
0
100
200
300
400
500

Fig. 9.

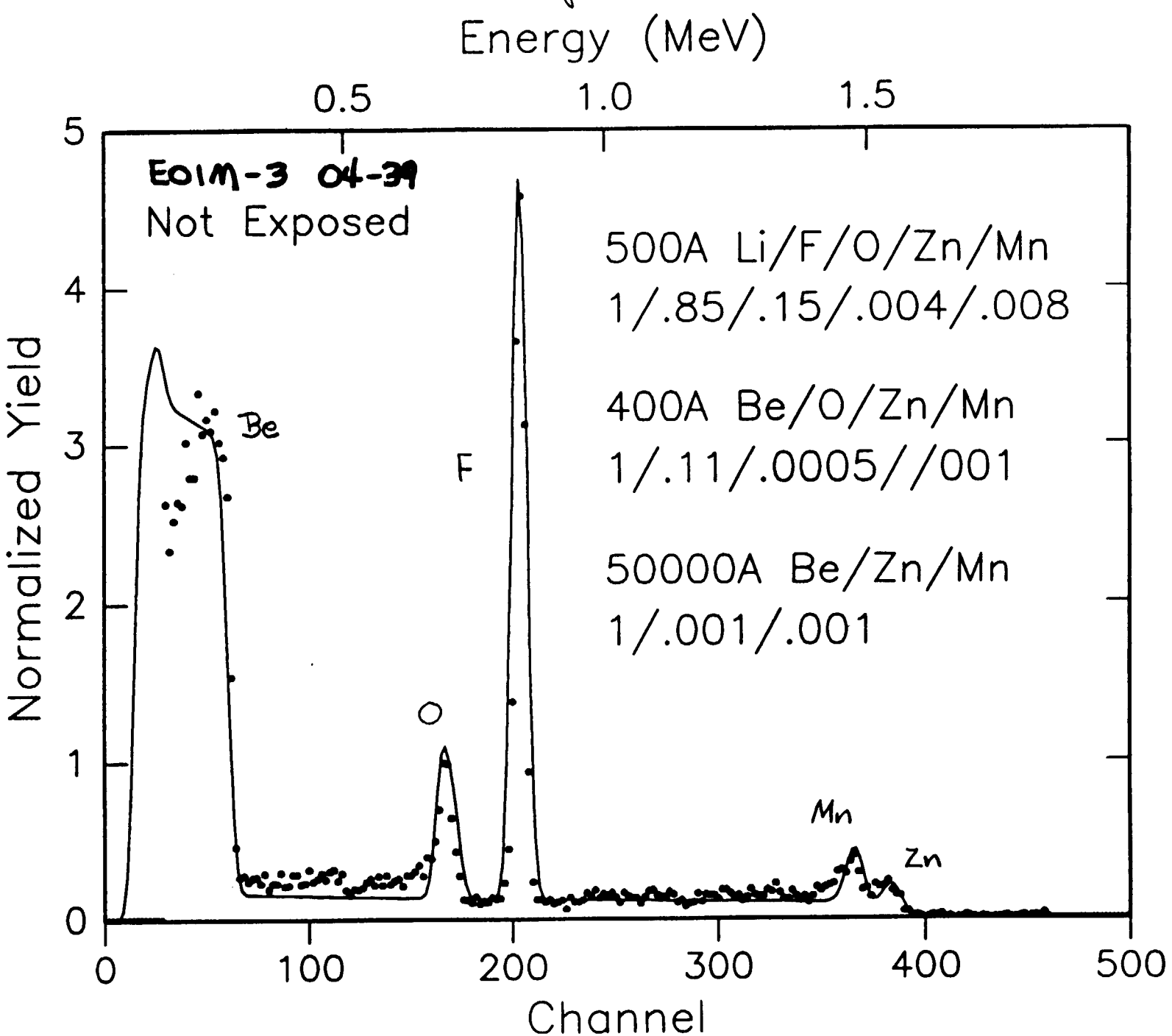
Energy (MeV)
0.5
1.0
1.5
EOIM-3 04-39
Not Exposed
500A Li/F/O/Zn/Mn
1/.85/.15/.004/.008
400A Be/O/Zn/Mn
1/.11/.0005//001
50000A Be/Zn/Mn
1/.001/.001
Be
O
F
Mn
Zn
Normalized Yield
0
1
2
3
4
5
0
100
200
300
400
500
Channel

Fig. 10.

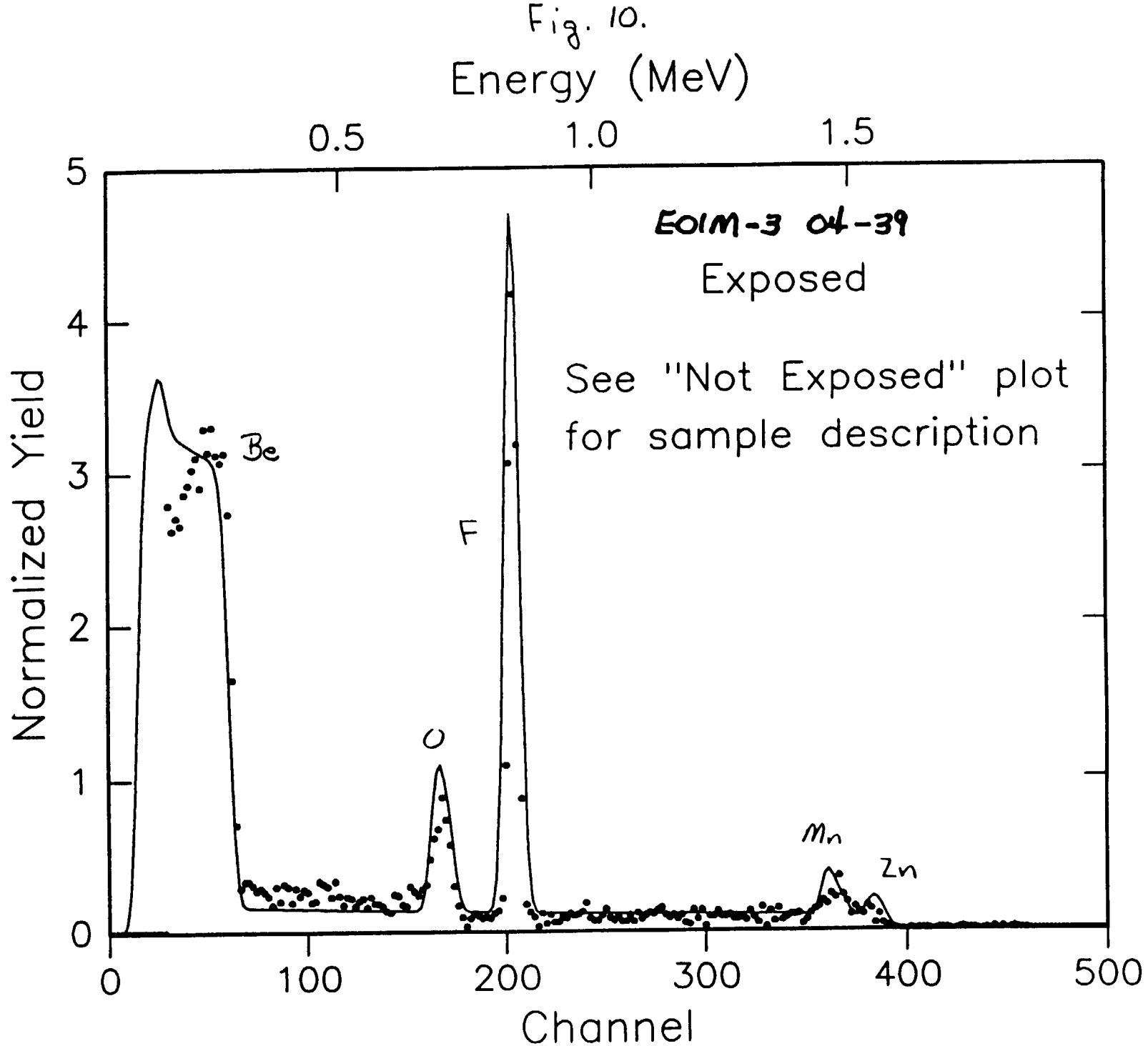
Energy (MeV)
0.5
1.0
1.5
EOIM-3 04-39
Exposed
See "Not Exposed" plot
for sample description
Be
C
F
Mn
Zn
Normalized Yield
0
1
2
3
4
5
0
100
200
300
400
500
Channel